Hewawasam, T., von Blanckenburg, F., Bouchez, J., Dixon, J. L., Schuessler, J. A., Maekeler, R. (2013): Slow advance of the weathering front during deep, supply-limited saprolite formation in the tropical Highlands of Sri Lanka. - Geochimica et Cosmochimica Acta, 118, 1, 202-230

DOI: 10.1016/j.gca.2013.05.006

Slow advance of the weathering front during deep, supply-limited saprolite formation in the tropical Highlands of Sri Lanka

Tilak Hewawasam[1*], Friedhelm von Blanckenburg[2], Julien Bouchez[2], Jean L. Dixon[2], Jan A. Schuessler[2], Ricarda Maekeler[2,3]

[1]Department of Natural Resources, Sabaragamuwa University of Sri Lanka, Belihuloya, Sri Lanka, tilak@sab.ac.lk.

[2]GFZ German Research Centre for Geosciences, Section 3.4, Earth Surface Geochemistry, Telegrafenberg, 14473 Potsdam, Germany fvb@gfz-potsdam.de

[3] DFGGraduate School 1364 at Institute of Geosciences, University of Potsdam, Germany

Geochimica Cosmochmica Acta 2013 doi:10.1016/j.gca.2013.05.006

Abstract

Silicate weathering – initiated by major mineralogical transformations at the base of ten meters of clay-rich saprolite – generates the exceptionally low weathering flux found in streams draining the crystalline rocks of the mountainous and humid tropical Highlands of Sri Lanka. This conclusion is reached from a thorough investigation of the mineralogical, chemical, and Sr isotope compositions of samples within a regolith profile extending >10 m from surface soil through the weathering front in charnockite bedrock (a high-grade metamorphic rock), corestones formed at the weathering front, as well as from the chemical composition of the dissolved loads in nearby streams. Weatherable minerals and soluble elements are fully depleted at the top of the profile, showing that the system is supply-limited, such that weathering fluxes are controlled directly by the supply of fresh minerals. We determine the weathering rates using two independent means: (1) *in situ*-produced cosmogenic nuclides in surface soil and creek sediments in the close vicinity of the regolith combined with immobile element mass balance across the regolith and (2) river dissolved loads. Silicate weathering rates determined from both approaches range from 16 to 36 t km^{-2} y^{-1}, corresponding to a weathering front advance rate of 6 to 14 mm ky^{-1}. These rates agree across the 10^1 to 10^4 y time scales over which our rate metrics integrate, suggesting that the weathering system operates at steady state. Within error these rates are furthermore compatible with those obtained by modeling the advance rate of the weathering front from chemical gradients and mineral dissolution rates. The silicate weathering flux out of the weathering profile, measured on small creeks, amounts to 84% of the profile's export flux; the remaining 16% is contributed by non-silicate, atmospheric-derived input. The silicate weathering flux, as measured by dissolved loads in large catchments, amounts to ca. 50% of the total dissolved flux; the remainder being contributed by dust, rain, and weathering of local marble bands. Spheroidal weathering is the key processes of converting the fresh bedrock into saprolite at the weathering front. The mineralogical composition of weathering rinds shows that the sequence of mineral decomposition is: pyroxene; plagioclase; biotite; K-feldspar. Observable biotite alteration does not appear to initiate spheroidal weathering within corestones; therefore, we infer that other processes than biotite oxidation, like pyroxene oxidation, clay formation from pyroxene and plagioclase decomposition, the development of secondary porosity by plagioclase dissolution, or even microbiologic processes at depth enable the coupling between slow advance of the weathering front and slow erosion at the surface. The comparison to tectonically more active tropical landscapes lets us conclude that the combination of hard rock with tightly interlocked mineral grains and slow erosion in the absence of tectonically-induced landscape rejuvenation lead to these exceptionally low weathering rates.

1. Introduction

A large part of the continental surface located in areas of tropical climate is characterised by geologic shield rock covered by thick saprolite and soil. It is important to document the weathering processes in these tropical environments since such settings have a large spatial contribution to global solute and sediment fluxes (Milliman and Meade, 1983; Meybeck, 1987) and the drawdown of atmospheric CO_2 by silicate weathering. We already know that weathering rates in low-relief tropical areas are low (Gaillardet et al., 1999a), and that one factor that limits the rates in these areas is the absence of relief that is otherwise a precondition for elevated erosion rates. However, this precondition is not universally valid: at least two settings have been described in which low erosion and weathering rates prevail in relatively steep, mountainous tropical watersheds: the Guyana Shield (Edmond et al., 1995) and the tropical Highlands of Sri Lanka (von Blanckenburg et al., 2004). The specific geologic condition that prevents more rapid erosion and simultaneous replacement of soils by weathering in such tropical mountain belts is still poorly understood as we lack understanding of the rate-limiting mechanism that prevents rapid soil production and erosion in these steep, wet, hilly terrains.

With regards to the cause for low erosion rates in shield terrains, the hypothesis was put forward that such rates are due to the lack of active tectonic processes that might lead to a geomorphic "rejuvenation" of the landscape and its subsurface hydrologic regime (Edmond et al., 1995, von Blanckenburg et al., 2004).A preliminary confirmation of this picture is emerging from the very few studies that present soil production rates in tropical humid settings. These settings commonly display similar saprolite thicknesses of roughly 10 to 20 m, but record different rates of saprolite formation. For a lateritic soil over granodiorite in the Nsimi catchment (Cameroon), chemical budgets resulted in a saprolite formation rate of 5 t km^{-2} y^{-1} (Braun et al., 2012) while in the south Indian Mule Hole catchment these rates were determined to be around 60 t km^{-2} y^{-1} (Braun et al., 2009). U series measurements involving the modeling of U gain and loss yielded a saprolite formation rate of 20 t km^{-2} y^{-1} for laterite formed over gneiss in Cameroon (Dequincey et al., 1999). Cosmogenic nuclides on soils in the tropical Highlands of Sri Lanka yielded denudation rates interpreted as soil production rates of 5 to 30 t km^{-2} y^{-1}(von Blanckenburg et al., 2004).(Note that for these estimates, all lowering rates have been converted using a density of 2700 kg m^{-3}. We furthermore do not include U-series rates from volcanoclastic lithologies (Dosseto et al., 2012) or early U-series measurements not taking loss of isotopes into account (Matthieu et al., 1995) in this comparison. However, a much faster saprolite formation rate was obtained in the Luquillo granodiorite (Puerto Rico); there, cosmogenic nuclides on soil yield 90 t km^{-2} y^{-1} (Riebe et al., 2003), and mass balance of stream and soil chemistry, Sr isotope mass balance, and U-series nuclides yield a range of 120 to 200 t km^{-2} y^{-1} (summarised in Chabaux et al., 2013). As Luquillo is located in a tectonically active setting, these higher rates lend support to the hypothesis of the tectonic driver to chemical weathering.

With regards to the rate-limiting mechanism of soil production, an increasing body of evidence suggests that the key process takes place at the weathering front, where fresh bedrock is converted into regolith (*e.g.* Anderson et al., 2002). Spheroidal weathering, the process that produces concentric, onion-skin type weathering rinds around bedrock corestones (Chapman and Greenfield, 1949), is an extensively explored process converting bedrock into weathered material, and thereby may set the advance rate of the weathering front in a wide range of settings (Sak et al., 2004, 2010; Fletcher et al., 2006; Royne et al., 2008; Buss et al., 2008). Several mechanisms have been suggested for spheroidal weathering, and most of these involve fracturing induced by local strain that is caused by several processes: 1) mineralogical transformations involving volume change such as the oxidation of ferrous minerals, mostly biotite (Fletcher et al., 2006; Lebedeva et al., 2007, Buss et al., 2008); 2) the precipitation of secondary minerals therein, thereby generating stress and fracturing (Røyne et al., 2008; Jamtveit et al., 2009, 2011); 3) or the utilization of mesofractures by fungal hyphae that supply water and mineral-dissolving reagents (Graham et al., 2010). The spacing of initial fractures bounding corestones (Fletcher and Brantley, 2010), and of those formed by positive strain during spheroidal weathering (Fletcher et al., 2006) have been identified

as a key control over the rate of weathering front advance. All these mechanisms allow for the penetration of water, protons and oxygen deeper into bedrock as weathering proceeds, and hence for the downward propagation of the weathering front and concomitant soil production.

The Sri Lankan Highlands appear to be representative of a setting characterised by slow weathering in tectonically quiescent tropical shield rock.The denudation rates of the area were explored in three earlier studies. Hewawasam et al. (2003) assessed the strong impact of land use on erosion through a comparison of river basin denudation rates from cosmogenic nuclides with erosion rates from river total loads. von Blanckenburg et al. (2004) presented denudation rates derived from cosmogenic nuclides in both unperturbed and perturbed catchments for the central Highlands of Sri Lanka covering diverse geomorphic settings. These rates, considered to represent "natural", pre-anthropogenic denudation rates due to their long averaging time scale (10^4 to 10^5 y) were shown to be relatively low (5 to 30 t km^{-2} y^{-1}) despite the presence of significant relief in the Sri Lankan Highlands. Vanacker et al. (2007a) found that only in the very steep catchments of the post-rifting southern escarpment of the central Highlands denudation rates were comparable to those found in similar settings (30-180 t km^{-2} y^{-1}). von Blanckenburg et al. (2004) also presented best estimates of silicate weathering rates in the central Highlands based on dissolved loads monitored in rivers following a preliminary approach for correction for non-weathering inputs. These silicate weathering rates were also low, which was attributed to the poor supply of fresh surfaces of minerals due to slow prevailing physical erosion (von Blanckenburg et al., 2004). These findings directed them to suggest that the role of climate in controlling weathering in the central Highlands of Sri Lanka is ineffective since landscape rejuvenation by tectonic processes, an important prerequisite for physical erosion, does not prevail there (von Blanckenburg et al., 2004).

As none of the previous studies in the Sri Lankan Highlands were directed at identifying weathering processes at the regolith scale, here we explore weathering intensities and fluxes in a deep regolith profile developed over charnockite lithology. We report weathering intensities and identify and quantify the mineralogical transformations that take place where bedrock is converted to regolith, using microscopic and x-ray methods, in combination with mass transfer coefficients and chemical depletion fractions throughout the regolith profile (Brimhall and Dietrich, 1987; Anderson et al., 2002).The chemical depletion fractions are coupled with cosmogenic nuclide derived-denudation rates (Hewawasam et al., 2003 and von Blanckenburg et al, 2004) to compute chemical denudation (e.g., Riebe et al., 2004; Dixon et al., 2009a) rates from the regolith profile. We make use of the large variability of Sr isotope ratios among minerals in chranockite (Burton and O'Nions, 1990) to quantify weathering gradients of primary minerals throughout the regolith from its Sr isotope composition. We combine the calculation of gradients in the degree of weathering (White, 2002) across weathering rinds of the corestone with published mineral-specific dissolution rates, to compute the propagation rate of the weathering front into the corestones. We derive silicate weathering rates at the scale of large (100's km^2) river catchments from their solute loads. We find that the derived rates agree over the range of 10^1 to 10^4 y time scales, and across spatial scales ranging from the regolith profile to that of large watersheds. Finally, we explore reasons for the low rates found, discuss the way the weathering front advances at depth and review the potential mechanisms explaining how this weathering front advance is coupled to physical erosion at the surface.

2. Field Site and Methods

2.1 Study site

The central Highlands of Sri Lanka are a hilly to mountainous landscape at 500 to 2500 m elevation, and feature markedly higher relief and mean catchment gradients (10-20°) compared to the surrounding low-elevation coastal plain (Figure 1A). Geologically, the central Highlands of Sri Lanka occupy a large proportion of the crystalline Highland Complex, which comprises metasediments (interbedded quartzite,

marble and metapelites), metabasites, and charnockites formed under granulite facies condition (Cooray, 1994). The gneissic rocks in the Highland Complex contain compositionally segregated bands of minerals that are highly foliated. In contrast, charnockite is a massive rock having tightly interlocked mineral grains that is jointed at the meter to decimeter scale. Formation of corestones can be observed as the first weathering mechanism that occurs in charnockites. Importantly, geological maps show that a large portion (approximately 50%) in the central Highlands of Sri Lanka is underlain by charnockite or charnockitic rocks.

Thick regolith, including both soil and saprolite, mantle most of the landscape, but bare bedrock is also exposed on slopes of escarpments and some hillcrests. No surface rejuvenation by neotectonics is documented in this area. The area is subjected to two monsoons; south-west monsoon (June to September) and north-east monsoon (December to February) and mean precipitation varies from 1000 to 5000 mm y^{-1}.

This study focuses on a deeply weathered regolith profile (>10 m; Figure 2A) located at 1753 m altitude and exposed along the road from Nuwaraeliya to Welimada on a new road cut bordering a 12 km^2 natural forest reserve consisting of pristine, mature, stable upper montane rain forest, close to the Hakgala Botanical Garden. The mean annual temperature and precipitation at Hakgala are 16°C and 2013 mm, respectively. The site is often wrapped in dense mist and the relative humidity changes from 66% to 86% during the day and 79-93% at night (Weerakkody and Parkinson, 2006a). Strong winds (12–14 km h^{-1}) prevail at Hakgala in June and July and can cause considerable damage to the natural forest ecosystem (Weerakkody and Parkinson, 2006a). The forest has a thick canopy with a height up to 20 m and hosts 97 tree species, of which 62 are endemic. Weerakkody and Parkinson (2006b) revealed that total litterfall at Hakgala is 6.6–8.7 t km^{-2} y^{-1} of which 77–83% is leaf litter. The mean standing stock of litter on the forest floor was found to be around 10 t km^{-2}, of which 72% is woody litter since the decomposition rate is higher for leaf litter than for woody litter.

The regolith at Hakgala is located on a hillslope and developed on charnockite lithology, a meta-igneous rock of acidic composition metamorphosed under granulite facies conditions. The rock features SiO_2 > 65% with plagioclase, K-feldspar and quartz as major, and orthopyroxene (hypersthene) and biotite as minor mineral components. The profile evolved through deep weathering of the bedrock extending to at least 10 m in depth. The uppermost layer of the regolith in this area is a red-yellow lateritic soil with a prominent A horizon which is typical for virgin forests (Weerakkody and Parkinson, 2006a). The mobile soil layer is well-mixed and ~ 60 cm thick. An upper saprolite horizon extending from the base of soil to 6 m depth is reddish and extensively weathered. The lower saprolite horizon is banded with whitish and yellowish thin layers. Massive, rounded blocks of charnockite in different sizes from a few cm to 50 cm in diameter remain within the lower saprolite, below a depth of 8 meters, as corestones (Figure 2).

2.2. Sampling

In October 2010, 2 soil and 23 saprolite samples (ca. 500 g each) were collected from a vertical section of the regolith, exposed as a fresh road cut during ongoing construction works. Five horizontal density cores (15 cm-long and 4.6 cm-diameter plastic core sleeves) were taken throughout the saprolite for density measurement. Approximately 10 m upslope from the regolith profile, 9 additional soil samples were collected about 1 m downslope of the lysimeter locations (see below) at3 parallel sub-sections within the 60 cm-thick soil zone using a soil corer, integrating over depth intervals from 0-20 cm, 20 - 40 cm, and 40 - 60 cm. The soil sub-sections were located about 1.5 m apart from each other in order to account for potential lateral variability. In addition, a combined soil sample for each depth interval was produced by mixing equal mass aliquots from each depth interval of three soil sub-sections. A corestone of about 30 cm in diameter (Figure 2C) was sampled from a depth of *ca.*830cm, and fragile weathering rinds (each ~1 cm thick, composing a package up to 10 cm) were preserved in transparent plastic foil during removal of

the corestone from the profile. Nine unweathered bedrock samples were taken beneath the regolith profile.

Five pre-acid cleaned suction lysimeters (Nylon tubes, diameter 32 mm, ecoTech, Germany) with polyamide porous membrane filter tips (0.45 µm-porosity) were installed in October 2010 at different depths (22, 36, 70 and 107 cm vertically from surface to the lysimeter tip) within the weathering profile for three days to extract pore water. An extended period of deployment would have been desirable but was not possible for logistic reasons. Lysimeters were located ~ 10 m upslope of the sampled weathering profile. The soil-saprolite interface where lysimeters were placed is apparently deeper than at the location of the sampled profile. Three creeks draining ecologically pristine catchments (>1 km^2, Figure 1C) adjacent to the regolith profile at Hakgala were sampled at three occasions (October 2010, February 2011, May 2011) during both base and storm flows. One of them had been sampled during a previous study in March 2000(von Blanckenburg et al., 2004). Water was filtered at the sampling site using 0.22 µm-porosity PSE filter membranes in a 500 mL vacuum filtration unit, and acidified to pH ~ 2 with distilled $HNO_3$for storage in acid-precleaned PE bottles. We also made use of previously published chemical analyses of water samples from 7 ''large'' rivers draining the central Highlands of Sri Lanka (Figure 1A): six large catchments (50-150 km^2) of Atabage Oya (AO), Belihul Oya (BO), Huluganga (HUG), Maha Oya (MO), Nilambe Oya (NO), Uma Oya (UO), and one trunk stream catchment (1167 km^2)at Peradeniya (M-PER), all part of the large river basin of the Upper Mahaweli Watershed (Figure 1A). These rivers were sampled over a complete hydrological cycle in 2001-2002. Catchments drained by the three small creeks are underlain only by silicate rocks whereas large catchments are underlain by silicate rocks with occurrences of discrete crystalline marble layers of 100-300 m in thickness (Figure 1B). These large catchments drain areas featuring both natural and cultivated vegetation. Sampling, analytical methods and results for the water samples collected in 2001-2002 are reported in von Blanckenburg et al. (2004). The discharge data available for the 6 tributaries and the main trunk, which were sampled in 2001 to 2002, were obtained from the Mahaweli Authority of Sri Lanka. The raw data is provided in supplementary Table S1.

2.3. Analytical methods

Sample treatment and analyses were carried out at the German Research Center for Geosciences (GFZ), Potsdam, Germany. Bedrock, saprolite, and soil samples were oven dried at 60°C, and representative aliquots of the samples were pulverized in an agate mill to < 60 µm-grain size. Powders were weighed and then heated for 5 hours at 600 °C. Loss on ignition (LOI) was recorded and the remaining powder was used for alkali fusion (Li-metaborate) to produce glass beads that were analyzed by X-ray fluorescence spectrometry (XRF, Panalytical Axios Advanced) for bulk chemical composition. Relative analytical uncertainties on the reported XRF data are about 0.5% for major elements and about 10% on trace elements. Powder X-ray diffraction analyses (Siemens D5000, Cu-Kα radiation) were performed for mineral identification on selected samples. The corestone sample, including its fragile, few cm-thick weathering rinds, was embedded in epoxy. A series of thin sections along the corestone radius were made from the unaltered dark core to the outermost, yellowish weathering rind (Figure 3). Weathering reactions in the corestone were inferred based on observations on thin sections under the polarizing microscope and using scanning electron microscopy (SEM, Carl Zeiss Ultra 55 Plus) combined with energy dispersive X-ray analysis (EDX) on µm-sized spots to obtain chemical compositions of minerals. The corestone was sampled at three different positions along a transect from core to rim by sawing. Upon pulverization, the bulk chemical composition of these samples was analyzed by XRF. The mineral abundances in the bedrock samples were determined both by point counting using an optical microscope and by using a CIPW norm calculation from XRF bulk chemical compositions.

For Sr isotope analyses, 50to 100mg weighed aliquots of powder from selected unweathered bedrock (n=2), corestone (n=3), saprolite (n=7) and soil (n=3) samples were digested in a HF-HNO_3 mixture in

Teflon bombs at 120°C. The yield of the digestion procedure was checked through the analysis of the resulting solutions by ICP-OES and comparison with XRF analyses. A few tens of µL of the digested sample solutions (containing 100 to 500 ng Sr) were successively loaded onto two chromatography columns (2 mL AG50-X8, Dowex, and 0.2 mL Sr-SPEC, Eichrom) for separation and purification of Sr. Purity of the eluted solutions was verified, and Sr yields were checked to be 100 ± 10%, both by ICP-OES. Sr isotopes ratios were measured by multicollector ICP-MS (Neptune Plus, Thermo Scientific) in static mode (^{86}Sr in the central Faraday cup,) using an APEX-Q (ESI) desolvation unit as the introduction system in combination with a "Jet"-sampler cone and a "X"-skimmer cone. Ion beam intensities between 0.1 and 0.2 nA were obtained on the major isotope ^{88}Sr (signals between 10 and 20 V, using a $10^{11}\Omega$ resistor), and isotope ratios were recorded over 20 cycles of 4s-integration each. Kr interferences on masses 84 and 86 and Rb interference on mass 87 were corrected for using ^{83}Kr and ^{85}Rb signals along with Kr and Rb isotopes ratios as measured at the beginning of the sequence. Instrumental mass fractionation on the ^{87}Sr/^{86}Sr ratio was corrected for using the measured^{88}Sr/^{86}Sr ratio and the natural ratio, taken as 0.1194. Each sample was measured three to six times during a session. The associated 2S.D. was in the range1-5 x 10^{-5} on the ^{87}Sr/^{86}Sr ratio, equivalent to that estimated on a longer-term basis using the Sr carbonate reference material NIST SRM 987, which was frequently measured to check the accuracy of the method (^{87}Sr/^{86}Sr = 0.71024).

Dissolved element concentrations in stream waters and soil pore waters (Na, K, Ca, Mg, and SiO_2) were measured by optical emission spectrometry (ICP-OES, Varian 720-ES). Precision and accuracy were assessed by repeated measurements of the water reference materials SLRS-5 (National Research Council, Canada) and SRM1640a (National Institute of Standards and Technology, USA). Replicate analyses over the course of this study show a reproducibility of 2% and comparison with certified concentration values indicate an accuracy of better than 8% for all elements analyzed in this study. Alkalinity and pH were measured at the sampling site using a portable photometer (Aqualytic AL400 Maxidirect).

2.4 Calculation of strain (ε),chemical depletion fractions (CDF), and mass transfer coefficients (τ)

The concentration of an immobile element (e.g., Zr, Ti or Nb) in the weathered material relative to the parent rock can be used to determine the volume change and mass loss during weathering (Brimhall and Dietrich, 1987). The strain (**ε**) is the relative volume change occurring during weathering. **ε** can be calculated from the parent and weathered material density (ρ_{parent} and $\rho_{weathered}$, respectively) and from the concentrations of an immobile element X_i in the parent and weathered material ($[X_i]_{parent}$ and $[X_i]_{weathered}$, respectively) (Brimhall and Dietrich, 1987):

$$\varepsilon = \frac{\rho_{parent}}{\rho_{weathered}} \cdot \frac{[X_i]_{parent}}{[X_i]_{weathered}} - 1 \qquad (1)$$

Unweathered bedrock is considered as being the parent material throughout this study, and weathered material is either saprolite or soil. When **ε** = 0, the weathering is isovolumetric; positive values of **ε** mean that the solid material expanded during weathering, while negative values indicate compaction.

The chemical depletion fraction (CDF; Riebe et al. 2003) records fractional mass loss in regolith due to chemical weathering:

$$CDF = 1 - \frac{[X_i]_{parent}}{[X_i]_{weathered}} \qquad (2),$$

where $[X_i]_{parent}$ and $[X_i]_{weathered}$ represent concentrations of an immobile element X_i in the parent and weathered material, respectively. When CDF = 0, no loss of soluble elements has occurred from saprolite or soil as compared to the parent material; a CDF > 0 quantifies the total fractional mass loss during weathering. In most granitoid lithologies, CDF does not exceed a value of 0.5 as a large fraction of the

primary Si is locked in insoluble quartz, and a substantial fraction of Si, Fe, and Al released from primary minerals is retained in clay minerals.

Elemental regolith profiles constructed by plotting elemental mass transfer coefficients (τ) as a function of depth from top to bottom of a vertical section are widely used to document the time-integrated weathering intensity and processes in regolith (Brimhall and Dietrich, 1987;Anderson et al.,2002). The mass transfer coefficient of element X is defined as:

$$\tau_X = \frac{[X]_{weathered}}{[X]_{parent}} \cdot \frac{[X_i]_{parent}}{[X_i]_{weathered}} - 1 \qquad (3)$$

Where $[X]_{weathered}$ and $[X]_{parent}$ represent concentrations of element X in the weathered and parent material, respectively. When $\tau = 0$, X has not been lost as compared to the parent material; when $\tau < 0$ or $\tau > 0$, there is elemental loss or gain of X during weathering, respectively; $\tau = -1$ means 100% loss of the element from parent to weathered material.

As justified in section 3.2, in this study, CDF and τ were calculated using Zr as the immobile element.

2.5 Denudation and weathering rates

Denudation rates measured by cosmogenic nuclides ($D_{measured}$) comprise the sum of mass lost at or near the Earth surface by both physical erosion and chemical weathering (von Blanckenburg, 2005). They are reported in units of either length per time (*e.g.* mm ky^{-1}) or in units of mass per area per time (*e.g.* t $km^{-2}y^{-1}$). In most cosmogenic nuclide studies, these two ways of reporting are converted from each other by using the density of bedrock removed (typically 2700 kg m^{-3}). Values of $D_{measured}$ were determined in the vicinity of the regolith profile in previous studies using concentrations of *in-situ*-produced ^{10}Be in quartz of surface soil and creek sediments (Hewawasam et al., 2003; von Blanckenburg et al., 2004). However, as shown in Dixon et al. (2009a), $D_{measured}$ calculated at sites with deep regolith does not take into account the mass loss through weathering beneath the cosmic ray adsorption depth (~60 cm for rocks and ~100 cm for soil), and therefore may underestimate total denudation rates. For such cases, the corrected total denudation rate (D_{corr}), the total of mass loss in soil and saprolite due to physical and chemical processes, is calculated from the measured cosmogenic nuclide derived denudation rates ($D_{measured}$) using the following relationship (Dixon et al., 2009a):

$$D_{corr} = D_{measured} \cdot \frac{[X_i]_{saprolite}}{[X_i]_{bedrock}} \qquad (4)$$

We used the average Zr (for X_i) concentration of bedrock at the regolith sampling location, and the average Zr concentration of all saprolite samples to do this correction.

A long-term weathering rate (W), the rate of mass loss in soil and saprolite due to chemical processes, can be calculated using the CDF and the total denudation rate (D_{corr}) from *in situ*-produced cosmogenic ^{10}Be according to Riebe (2003):

$$W = CDF \cdot D_{corr} \qquad (5)$$

2.6 Determination of silicate weathering end members in dissolved loads from regolith chemistry

The pore water chemistry of the saprolite (end member of deep-seated weathering) could not be measured directly. Deep pore water element ratios were therefore inferred as follows. Assuming steady state, the flux of a soluble element X into deep pore water $F(X)_{diss}^{deep}$, integrated over the time scale of formation of

deep saprolite, is equal to the rate(per unit area) at which this element enters the weathering zone in parent rock multiplied by the fraction of this element lost during conversion of bedrock to saprolite. The fraction of element lost is quantified by the opposite of the elemental mass transfer of the deep saprolite, $-\tau_x^{deep}$. The rate at which an element contained in parent rock enters the weathering zone can be calculated by multiplying the concentration of that element in parent rock $[X]_{parent}$ with the rate at which bedrock is converted into deep saprolite. This rate can be assumed to be equal to denudation rate D_{corr} at steady state (Dixon et al., 2009a).Hence the time-integrated dissolved flux can be calculated:

$$F(X)_{diss}^{deep} = D_{corr} \cdot [X]_{parent} \cdot \left(-\tau_X^{deep}\right) \qquad (6)$$

Over the long term, this elemental flux is equal to the water flux flowing through the deep saprolite multiplied by the time-integrated concentration of *X* in this water pool, $[X]_{diss}$. Therefore:

$$F(X)_{diss}^{deep} = Q \cdot [Xdeep]_{diss} \qquad (7)$$

The same equations can be derived for a second element Y. Then, elemental solute ratios can be calculated for the elements X and Y from saprolite compositions:

$$\left(\frac{X}{Y}\right)_{diss}^{deep} = \frac{[X]_{parent}}{[Y]_{parent}} \cdot \frac{\tau_X}{\tau_Y} \qquad (8)$$

Note that the time-integrated fluxes described by eq. (6) and (7) will in many cases deviate from dissolved fluxes measured today. First the dissolved fluxes will fluctuate around a long-term mean, and an instantaneous dissolved flux measurement will yield data that will be subject to that fluctuation. In contrast, the loss ratios expressed by equation (8) describe time-integrated dissolved loss ratios. Second, dissolved loads also integrate inputs from the upper layers of the regolith profiles and from lateral inputs, whereas the loss ratios from equation (8) predict the pure deep porewater end-member. We show below that these ratios are consistent with the arrays described by measured dissolved loads, and are hence likely representative of long-term steady state flux ratios.

2.7Calculation of mineral weathering rates, propagation rate of the weathering front, and weathering gradients

Across a weathering front, mineral weathering rates (R_{min}, in $mol_{min}\ m^{-2}{}_{min} y^{-1}$, where *min* is *Pl* for plagioclase, *Bt* for biotite, *Kfs* for K-feldspar and *Px* for pyroxene) are linked to the rate of advance of this weathering front *w* (m y^{-1}) *via* the "weathering gradient" of an element *X* ($\Delta[X]/\Delta z$, in $mol_X\ kg^{-1}{}_{rock}\ m^{-1}$, units are modified from White (2002)) by:

$$R_{min} = \frac{\omega}{S_{min} \cdot x_{min,r} \cdot \beta} \cdot \frac{\Delta[X]}{\Delta z} \qquad (9)$$

Where S_{min} is the mineral-specific surface area (in $m^2{}_{min}\ g^{-1}{}_{min}$), $x_{min,r}$ is the mass proportion of the considered mineral in the source rock (in $g_{min}\ kg^{-1}{}_{rock}$), and β is the molar proportion of *X* in the considered mineral (in $mol_X\ mol^{-1}{}_{min}$). In section 4.2, equation9is solved for *w* using weathering gradients of Na and Ca, reflecting that of plagioclase, across the weathering front displayed in the corestone.

If the mineral proportions are available, the element concentration gradient in eq. (9) can be replaced by a mineral concentration gradient $\Delta C_{min}/\Delta z$, in $mol_{min}\ kg^{-1}{}_{rock}\ m^{-1}$ with:

$$\frac{\Delta[X]}{\Delta z} \cdot \frac{1}{\beta} = \frac{\Delta C_{min}}{\Delta z} \qquad (10)$$

In section 4.2, equation10is solved for *w* using the weathering gradient of biotite across the weathering front displayed in the corestone, and the weathering gradient of K-feldspar in the regolith.

2.8 Mixing equations for Sr

The concentrations of Sr and its isotope ratio ($^{87}Sr/^{86}Sr$) can be used to trace weathering of minerals in regolith (*e.g.*Blum and Erel, 1997). Given the mineral composition of the Hakgala charnockite and weathering profile (see sections 3.2 and 3.4) and assuming that Sr is not retained in secondary precipitates, the Sr mass and isotope budgets can be written for the bulk bedrock or weathered material:

$$[Sr]_{bulk} = \sum_{min}\left(x_{min,bulk} \cdot [Sr]_{min}\right) \qquad (11)$$

$$\left(\frac{^{87}Sr}{^{86}Sr}\right)_{bulk} = \sum_{min}\left(x_{min,bulk} \cdot \frac{[Sr]_{min}}{[Sr]_{bulk}} \cdot \left(\frac{^{87}Sr}{^{86}Sr}\right)_{min}\right) \qquad (12),$$

with *min* = *Pl*, *Bt*, *Px* or *Kfs*, since quartz does not contain any Sr. $[Sr]_{min}$ and $(^{87}Sr/^{86}Sr)_{min}$ is the Sr concentration (in $g_{Sr}\ g^{-1}{}_{min}$) and isotope composition in the considered mineral, respectively.$[Sr]_{bulk}$ (in $g_{Sr}\ kg^{-1}{}_{bulk}$) and $(^{87}Sr/^{86}Sr)_{bulk}$ are the Sr concentration and isotope composition in the bulk solid (rock or weathered material), respectively, and $x_{min,bulk}$ are mineral proportions (in $g_{min}\ kg^{-1}{}_{bulk}$) in bulk rock or weathered material. The bulk Sr concentrations and isotope composition are known for the Hakgala rock and weathering profiles (Tables 3,4 and 5), and mineral-specific Sr concentrations and isotope compositions are taken from Burton & O'Nions (1990). In section 4.2, equations 11and 12are solved for x_{Bt} in the Hakgala corestone and for x_{Bt} and x_{Plg} in the regolith.

3. Results: Chemical and mineralogical compositions and weathering rates

3.1. Mineralogical composition

According to point counting and CIPW calculation, the local charnockite bedrock is principally composed of K-feldspar (32%), quartz (30%) and plagioclase (25%). Biotite (7%) and orthopyroxene (4%) are minor mineral constituents; ilmenite, magnetite, apatite, allanite, and zircon appear as accessory minerals. This composition is comparable to the Kurunegala charnockite in the northwestern Sri Lanka (Burton and O'Nions, 1990)(Table 1).

XRD and microscopic investigations of the lower saprolite reveal the presence of primary quartz, biotite, K-feldspar, plagioclase, as well as the weathering products goethite and kaolinite (Table 2, Figure 3). Only quartz, goethite, and kaolinite were detected in the upper saprolite and soil.

3.2 Chemical composition of bedrock and choice of the immobile element

Elemental concentrations of the local bedrock at Hakgala, average concentrations of other charnockite outcrops at Kurunegala, Sri Lanka (Hansen et al., 1987; Burton and O'Nions, 1990), and average concentration of pelitic and psammopelitic granulites in the southwestern Sri Lanka (Prame and Pohl, 1994) are listed in the Table 3. All major and trace elements measured in the 9 samples collected from local bedrock at Hakgala show uniform concentrations, *i.e.*, standard deviations of the average are generally below 10%. This chemical homogeneity of the bedrock meets one of the conditions required for accurate calculation of CDF following equation 2. Figure 4 illustrates the relationship between three supposedly immobile elements (Zr, Ti and Nb) within soil, saprolite, local bedrock charnockite and charnockite at Kurunegala. In this diagram the weathering enrichment line, obtained by averaging elemental ratios of the local bedrock, describes the relationship expected for these elements' concentration in the regolith if they are fully immobile during weathering reactions, and if weathering

alone controls their changing concentrations. Both Nb and Ti are enriched relative to Zr in the soil and saprolite samples and Nb/Zr and Ti/Zr ratios deviate from that of bedrock, showing that dissolution of rock-forming primary minerals alone does not control the concentrations of Zr, Ti, and Nb. This deviation suggests either addition of Ti and Nb to the regolith profile, or loss of Zr, or a combination of both. At Hakgala, Ti might be enriched in topsoil due to external inputs (see section 4.3) followed by translocation downward into the saprolite because of the mobility of fine-grained minerals in weathering horizons (Cornu et al., 1999). Alternatively, Zr might be solubilised from zircons under extreme weathering conditions (Delattre et al., 2007). In order to identify the most likely scenario for the Hakgala weathering profile, we examine the relative volume change, or strain (ε), occurring during weathering (equation 1). Strain calculated from Zr concentrations (ε_{Zr}) increases monotonously from nearly 0 (meaning isovolumetric weathering) for the deepest saprolite sample to around 0.5 (50% expansion) in the upper saprolite at 2 m-depth, and finally reaches 0.8 in top soil (Table 6). Strain calculated from Ti concentrations (ε_{Ti}) is lower than 0.15 throughout the saprolite, except at 4 m-depth (Table 6). The fact that ε_{Zr}, unlike ε_{Ti}, (1) exhibits a monotonous, increasing trend from deep saprolite to top soil, (2) demonstrates isovolumetric weathering near the weathering front, where the weathering intensities are the lowest (see section 3.3), and (3) shows the highest strain values in the top soil, compatible with our own direct observations (high porosity and root density), suggests that ε_{Zr} yields the most reliable strain values and that Ti is significantly affected by external inputs. Finally, the choice of an immobile element over another should also be motivated by the precision that can be obtained on its bedrock concentration. Nb is present in the bedrock in trace levels (about 11 to 39 ppm) close to the detection limit (10 ppm) of the XRF measurements and hence its concentration data are associated with high uncertainties. Zr concentrations in the bedrock samples from Hakgala show the smallest variability (relative standard deviations are 6.7% for Zr, 9.6% for Nb and 8.3% for Ti, Table 3). Considering all aspects, Zr appears to be the best-suited immobile element. Hence, we use Zr for the calculation of weathering indices in this study.

3.3 Chemical composition, depletion, and enrichment of saprolite and soil

Elemental concentrations in soil and saprolite are listed in Table 4. A significant variability in CDF is observed within the regolith profile (Table 4). Saprolite chemical depletion fractions (CDF, calculated using Zr as the immobile element; equation 2) index chemical mass loss during bedrock to saprolite conversion and increase from 0.1 to 0.6 upward from the saprolite-bedrock interface at 10.2 meters to the soil-saprolite boundary at a depth of 0.6 m (Figure 5). The upward trend of increasing CDF shows a gradual increase of the intensity of saprolite weathering and associated mass loss towards surface within the saprolite zone. These data show that up to 60% of the original rock mass is lost through chemical weathering in saprolite.

Elemental depletion profiles (τ-plots, using Zr as immobile element according to equation 3) were constructed for the entire profile. To confirm the choice of Zr over Ti as immobile element (section 3.2) we also explored whether the use of Ti as immobile element results in different τ-patterns than when using Zr, and found that except for certain elements like Al and Fe that are enriched in the topsoil the difference in patterns is negligible. Using Zr as the immobile element (Figure 6), it is apparent that Ca and Na are entirely depleted throughout the regolith section from the saprolite-bedrock boundary to the surface (Figure 6A and B). Sr, Mg, K, P and Si show an increasing trend of depletion towards the surface of the regolith. Al and Mn suffer minor loss within the saprolite, but exhibit τ-values of -0.5 in the soil. Only Fe and Ti do not show any evidence for loss, and both are in fact enriched in the surface soil relative to bedrock. In addition, Mg, Ca, Sr, and to a lesser extent Rb show significant enrichments from the upper boundary of the saprolite to the mobile soil layer immediately above it (Figure 6).

3.4 Chemical and mineralogical composition of the corestone and weathering rinds

The sampled corestone is a single-piece ellipsoid (ca. 30 cm long and 20 cm wide) with a dark, apparently fresh, charnockite core (zone 1), mantled by a 2 to 3 cm-thick white zone (zone 2) and a 0.5 to 1 cm-thick yellow-brown zone, most likely enriched in oxides (zone 3, Figure 3A). The corestone is surrounded by several partially disaggregated, yellow, cm-scale layers called "weathering rinds" (zone 4).

A complete description of the textural, mineralogical and chemical changes occurring from the unweathered core to the outer weathering rinds is beyond the scope of the present work and will be carried out in further studies. However, preliminary SEM and EDX observations reveal no weathering features in the dark core of the corestone (zone 1), although orthopyroxenes display significant fracturing and intra-mineral porosity (Figure 3B). In zone 2, alteration features were observed on pyroxenes as dark-grey bands within intra-mineral fractures (Figure 3C). Other minerals remain apparently unweathered in this layer. In zone 3, the outer rim of plagioclase grains as well as a thin layer along intra-plagioclase grain fractures (Figure 3D, E), are altered to relatively Na- and Ca-poor material. In the outermost weathering rinds (zone 4), plagioclases are highly fractured and thin structures, mostly composed of Al, Si and Fe, are visible in voids (Figure 3E). Pyroxenes display large altered regions of low apparent "relief" that are depleted in Mg and Mn as compared to unweathered regions of the grains (Figure 3F). Biotite show intertwined darker layers in back-scattered electron (BSE) images depleted in K, Mg, and Fe and enriched in Al and Si as compared to grey, fresh biotite layers (Figure 3D). Quartz and accessory minerals remain unweathered throughout the whole corestone, while K-feldspars display small dissolution pits along exsolution lamellae, but no significant volume loss.

Despite mineralogical changes in the three corestone zones, bulk XRF analyses show that the bulk mass loss as characterised by CDF is very low (Table 4 and Figure 5) in the corestone. However, individual elements like Na, Mg, Mn, and Ca show variable depletion of up to 40, 30, 75, and 45%, respectively from the unweathered core to the weathering rinds (Figure 6).

3.5 Sr isotopes

Sr isotope ratios ($^{87}Sr/^{86}Sr$) in charnockite bedrock bulk samples are 0.737-0.739 (Table5, Figure7). Burton and O'Nions (1990) report Sr concentrations and isotope composition along with mineral modes allowing us to estimate that the major Sr-carrying mineral phases in charnockite at Kurunegala are plagioclase (47% Sr), K-feldspar (53%) and biotite (0.34%), with $^{87}Sr/^{86}Sr$ ratios of 0.715, 0.732 and 5.13, respectively. From these numbers, a bulk $^{87}Sr/^{86}Sr$ ratio of 0.740 can be computed for the bulk charnockite at Kurunegala. Orthopyroxene can be ignored in this budget since only 0.05% of rock Sr is hosted in this mineral, with an isotope ratio of 0.726, close to that of bulk rock. This bulk rock ratio from Kurunegala is close to our measured $^{87}Sr/^{86}Sr$ for bulk unweathered charnockite at Hakgala (0.737-739) or for zone 2 of the corestone (0.740). This similarity suggests that the Hakgala weathering profile is indeed representative of the Sri Lankan Highlands. Sr isotope ratios increase outward in the corestone, from 0.740 in zone 2 to 0.747 in the outer rind (zone 4). A consistent increase in $^{87}Sr/^{86}Sr$ throughout the saprolite is observed, with values starting from 0.745 at 10 m-depth and reaching 0.764 at 4 m-depth (Table 5, Figure 7). The$^{87}Sr/^{86}Sr$ ratios in soils and the uppermost 50 cm of the saprolite are much lower than at other depths within the weathering profile, with values of 0.718-0.719 above 0.6 m-depth, and around 0.729 at 1 m-depth (Table5, Figure7).

3.6 Weathering and denudation rates

Cosmogenic nuclide-derived denudation rates have previously been reported by Hewawasam et al. (2003) and von Blanckenburg et al. (2004). In the vicinity of the regolith profile these rates vary from 7.9 to 11.4 mm ky^{-1}, averaging at 10.3 ± 1.4 mm ky^{-1} (Table 6). These reported rates underestimate the total denudation across the entire regolith since the latter includes a zone of deep saprolite and hence features mass loss beneath the depth of cosmogenic nuclide production (Dixon et al., 2009a). We use equation 4to

determine a denudation rate corrected for this effect. The ratio of averaged Zr concentration between saprolite (averaging 21 samples collected from 1 m depth to 10.2 m depth excluding one outlier) and bedrock (averaging the 9 bedrock samples) is 1.5. The total denudation rate across the entire regolith is thus 15.5 mm ky^{-1}. By multiplying this total denudation rate with average CDF for bedrock to soil conversion of 0.5 (equation 5), a weathering rate of 8 mm ky^{-1} for the10^4 y time scale can be constrained for this profile, corresponding to ~ 21 t km^{-2} y^{-1} (Table 7).

3.7 Water chemistry

Concentrations of dissolved species in soil water are variable and do not follow a consistent trends with sampling depth (Table S2). SiO_2 is the major dissolved species in soil water, and small creeks and large catchment river water (Table S2). Although the three sets of small creek samples were taken under different hydrological conditions, their chemical composition remains relatively constant (except for the HAK-2011-S3-3 sample, which might have been contaminated by fertiliser or domestic waste, as witnessed by its high Ca/Na and Mg/Na ratios, Table S2, and see section 4.4.2). The rather constant chemical composition indicates that the weathering system drained by these small creeks behaves chemostatically (Godsey et al., 2009). Such a chemostatic behavior is also observed at the scale of the seven larger rivers sampled in 2000-2001, in which the temporal variability in SiO_2, Na, K, Ca, and Mg concentrations is much lower than the variability in discharge (Table S1). This chemostatic behavior indicates that the measured chemical composition of creeks and large rivers is representative of longer-term (10^0-10^1 y) fluxes.

The total cationic load of the small creeks, in which we include SiO_2 here, is between 7.2 and 43.6 mg L^{-1}, whereas it spans a range of 23 to 64mg L^{-1} (rivers HUG and UO, respectively) in large catchment rivers. The corresponding cationic yields are between 35 and 67 t $km^{-2}y^{-1}$ (rivers NO and MO, respectively) (Table 7).

4. Discussion

4.1 Processes of conversion of bedrock to saprolite

Mineral grains in the charnockite bedrock are tightly interlocked and not foliated as commonly visible in gneissic rocks. A pathway to allow water and chemically reactive fluids to access the charnockite bedrock is present in the form of several sets of macroscopic joints. These are visible within the local bedrock as well as in the nearby charnockite outcrops along the Nuwaraeliya-Welimada road. Rocks in Sri Lankan basement are deformed under brittle conditions (Kehelpannala et al., 2006; Emmel et al., 2012). Such initial weathering along the pre-existing joint planes has formed corestones, which were then subjected to spheroidal weathering (Linton, 1955; Ollier, 1971;Mulyanto et al., 1999; Sak et al., 2010).

SEM observations of the corestone indicate that pyroxene is the first mineral affected by alteration in zone 2 (Figure 3), followed by plagioclase and biotite in zone 3. Secondary products of the weathering of pyroxene are present in significant amounts in zones 3 and 4, and those of plagioclase and biotite only within zone 4. However, despite these mineralogical transformations, no significant fractional mass loss occurs throughout the three zones, as shown by CDF (Table 4 and Figure 5). Only Na, Mg, Mn, and Ca feature some loss within the rind zone (Figure 6), suggesting dissolution of plagioclase and pyroxene. Accordingly, weathering of plagioclase and subsequent solubilization of Sr with a low isotope ratio is likely to lead to the observed trend of upward increasing $^{87}Sr/^{86}Sr$ (Figure 7). However, it can be estimated using equation 12 that if plagioclase were the only mineral decomposing in the corestone, much higher $^{87}Sr/^{86}Sr$ ratios (*i.e.* between 0.8 and 1) would be obtained in the weathered residuum. This observation indicates that ^{87}Sr-rich Sr is released from the solid, which could be accounted for by biotite oxidation and subsequent release of small amounts of radiogenic Sr from the crystal lattice (Blum and

Erel, 1997). In section 4.2, we use Sr isotope ratios to estimate the propagation rate of the weathering front in the corestone.

About 10 to 30%of mass is lost within the saprolite immediately above the weathering front. Further progressive elemental depletion occurs throughout the saprolite profile, amounting to as much as 50 to 60% just beneath the surface soil layer at 0.1-0.2 m depth (Figures 5 and 6). Elemental depletion in the vertical saprolite profile follows a sequence of Ca = Na; Sr; Mg; K; P = Rb; Si; Al. The τ plots show that Ca and Na, while mostly preserved within the rind zone, are fully depleted immediately above the regolith weathering front. In the charnockite bedrock, these two elements are mostly contained within plagioclase. Hence, their loss is mineralogically controlled by plagioclase weathering. Furthermore, no secondary minerals containing these elements, such as Na- or Ca-smectite, were detected by XRD or SEM analyses, indicating effective Na and Ca export in the dissolved form. XRD analyses explain the stronger depletion of Ca and Na as compared to K and Mg by the presence of residual biotite in the saprolite. Finally, although K-feldspar grains remain relatively unweathered in the corestone, they are fully decomposed at the top of the saprolite profile, resulting in almost complete depletion of Rb and K. As discussed above for the corestone, the upward increase in $^{87}Sr/^{86}Sr$ throughout the saprolite from 10.2 m- to 3 m-depth (Fig. 7) shows the increasing relative contribution of residual biotite to the Sr-budget, which again indicates the persistence of biotite in the saprolite while K-feldspar and pyroxene are being weathered virtually to completion. Only the depletion pattern of Si and Al are controlled to a large degree by the formation of kaolinite and its re-dissolution at the top of the profile (Figure 6D).

Combining observations within the corestone and the elemental depletion patterns in the regolith profile, the following sequence of mineral susceptibility to weathering of charnockite in tropical settings can be proposed: orthopyroxene; plagioclase; biotite; K-feldspar; apatite; quartz. That pyroxene alteration precedes that of biotite is important here, as previous work on other tropical weathering in Puerto Rico suggested biotite oxidation and the associate positive volume change may be the driver for the propagation of the weathering front (Fletcher et al., 2006, Buss et al., 2008). Furthermore, analyses here suggest that biotite alteration in the Hakgala charnockite follows initial plagioclase weathering. In contrast to what is shown in other tropical weathering profiles by Buss et al. (2008), plagioclase weathers before and faster than noticeable biotite alteration takes place. Therefore the primary control on the conversion of bedrock to saprolite appears to be either an increase in secondary porosity by initial pyroxene and plagioclase dissolution (Sak et al. 2010; Navarre-Sitchler et al, 2011), or the formation of fractures by a positive volume change associated with the formation of clays from these primary minerals (Røyne et al., 2008; Jamtveit et al., 2009; Jamtveit et al., 2011) or the oxidation of iron (II) in pyroxene.

4.2 Rate of weathering front advance

White (2002) suggests a method to calculate mineral weathering rates and the rate of propagation of the weathering front (equation 9) from observed weathering gradients. We note that this approach is strictly valid in one-dimensional systems such as ridgetops, whereas our site is located on a hillslope. Hence, slope-parallel transport and ensuing displacement and precipitation of solutes can potentially bias our results by locally enriching the profile in small-scale precipitates. We have no means to quantify this bias, but we assume that it is smaller than the uncertainty introduced by mineral dissolution rates used. We first solve equation 9for *w* in the Hakgala corestone based on the weathering gradients of Ca and Na (Table 8). Since in the Hakgala charnockite all Ca and almost all Na are carried by plagioclase, the depletion of these elements from the corestone center to the outward rinds reflects plagioclase dissolution. The calculation yields a weathering front propagation rate in the corestone of between 0.14 and 19 mm ky^{-1}, with the best estimate being around 2 mm ky^{-1}.Since biotite also decomposes in the corestone, a similar calculation can be made using Sr isotopes to infer biotite depletion across the corestone, and biotite weathering rates (equation 9). We calculate a rate for the corestone weathering front propagation of *ca.* 0.06mm ky^{-1} (between 0 and 0.6 mm ky^{-1}, Table 8) using published biotite dissolution rates and 48 mm

ky^{-1} using the biotite oxidation rate instead. The propagation rate of the corestone weathering front derived from the biotite weathering gradient therefore overlaps with that calculated from the plagioclase weathering gradient. Finally, the same principle can be applied to the regolith profile using the K-feldspar weathering gradient in the saprolite. Indeed, the progressive depletion of K and Sr in the saprolite (Figure 6) is compatible with K-feldspar being weathered throughout the regolith, and Sr isotopes can be used to quantify K-feldpar loss (Table 8). A regolith weathering front propagation rate of ca. 5 mm ky^{-1} (between 0.4 and 43 mm ky^{-1}) is obtained from equation 9 (Table 8).

The best estimates for the "corestone weathering rate", between 0.1 and 50 mm ky^{-1}, are similar to the calculated propagation rate of the weathering front at the regolith scale (5mm ky^{-1}) and the denudation rate inferred from CDF and *in-situ*-produced cosmogenic ^{10}Be (15.5 mm ky^{-1} see Table 7). However, we note that the lower end of these estimates points at distinctly slower dissolution rates at the corestone scale than at the regolith scale. At the current state of knowledge, this difference is still obscured by the large uncertainties introduced by the mineral dissolution rates used. If this difference were shown to be valid, then a likely explanation is the relatively larger surface area of the weathering front at the corestone interface scale as compared to the hillslope area governing the advance rate at the regolith scale. In other words, to maintain the same weathering fluxes at both scales, the rate of propagation of the weathering front (normalized to its surface area) has to be lower at the mineral scale (Navarre-Sitchler and Brantley, 2007; Ma et al., 2012).

4.3 Enrichment and mixing trends of elements in topsoil

In the Hakgala weathering profile, the 0.6 m-thick top soil show chemical and Sr isotope compositions that are undoubtedly distinct from the rest of the profile: (1) Mg, Ca, Al, Si, Ti are enriched relative to saprolite just beneath the soil (Figure 6) and (2) Sr isotope ratios are much lower than in unweathered rock and saprolite (Figure 7). (We note that the uppermost saprolite sample features relatively lower Sr isotope ratio too when compared to the saprolite sample beneath it. We explain this lower ratio as the result of contamination by soil material (by natural mixing processes or accidentally during sampling)).

Although Ca and Mg are important nutrients, their enrichment in the Hakgala soil cannot be the result of "nutrient uplift" by plants, occurring when plants preferentially extract elements from the weathering profile that are then recycled into the top soil through litter fall (Jobbágy and Jackson, 2004). Indeed, nutrient uplift cannot explain the enrichment of Al and Ti, as these are not chemical elements essential to plant growth, nor would nutrient uplift result in lower $^{87}Sr/^{86}Sr$ ratios as, for these isotope ratios, mass-dependent fractionation is corrected for during measurement and data treatment. Furthermore, the nutrient uplift model predicts an enrichment of K, the major metal nutrient. Such an enrichment of K is not observed.

The low Sr isotope ratios measured in topsoil of the Hakgala weathering profile rather suggest an external source. These low Sr isotope ratios are compatible with those prevailing in carbonate material. Moreover, using the concentration data reported in Table 4, it can be calculated that Ca and Mg concentrations increase from the upper saprolite to those found in soil by ca.1700 and 750 ppm, respectively. Carbonate bands, mostly of dolomitic composition, are present in the sampling area (Figure 1). Ca and Mg-rich material could thus be supplied from upslope areas by soil creep. However, this hypothesis fails to explain the enrichment of Al and Ti observed in the soil. Two other processes are able to supply the top of the weathering profile with carbonate-rich, silicate-bearing solid material: (1) local dust from fertilizers rich in dolomitic marble, which also contains silicate material, or (2) dust from either regional or global emissions.

Concerning hypothesis (1), dolomitic marble is widely used as a powdered rock fertilizer in tea estates of the central Highlands to reduce soil acidity and also as Mg fertilizer. Locally produced powdered rock

phosphate (Ca-phosphate) is also applied in the tea estates as a P fertilizer (Dahanayake et al., 1995). Even though the Hakgala location was never used for agriculture, powdered fertilizer applied in nearby plantations might have been distributed by monsoonal winds and added to the surface soil as a local dust. However, these sources have much higher Ca/Mg ratios than that observed in Hakgala topsoil (Dahanayake, 1995; Pitawala et al., 2003), suggesting that different Ca- and Mg-rich sources preferentially contribute to the regolith profile, such as dust from regional or global emissions.

In support of hypothesis (2), Sr isotope ratios reported by Grousset & Biscaye (2005) for North African, Asian and Southern Hemisphere dusts are indeed compatible with the isotope ratios measured in top soil (Figure 7). However, no study has as yet identified potential dust inputs into the Sri Lankan Highland, its source, mode of transport and deposition. It is commonly believed that the widespread distribution of red earth deposits on the coastal plain in Sri Lanka, especially in the Jaffna peninsula, is aeolian in origin. According to the *Dirtmap* data base (www.bridge.bris.ac.uk/projects/DIRTMAP) (Kohfeld and Harrison, 2001), a flux of 5-10 t km^{-2} y^{-1} of dust has been measured in marine sediments a few thousand kilometers west of Sri Lanka for the late Holocene and the Last Glacial Maximum. Assuming that the high elevations of Sri Lanka are being subject to a flux of this magnitude, the input represents ca. 25-50% of the total denudational flux. Such input could have a considerable impact on soil mineralogy, and soil and river geochemistry. We can estimate the dust flux balancing denudation that is required to explain the topsoils' Ca and Mg concentrations. Considering a soil density of 1.1 g cm^{-3}(Table 6) and using the observed soil depth of 60 cm, the increase of Ca and Mg from upper saprolite to topsoil corresponds to an additional inventory of 1.2 and 0.5 kg m^{-2} of Ca and Mg, respectively. The residence time of topsoil in Hakgala being around 75 ky (computed by dividing the soil depth of 60 cm by the erosion rate of 8 mm ky^{-1}, Table 7), the required input rates of Ca and Mg are 0.016 and 0.007 t km^{-2} y^{-1}, respectively. For these, addition rates of Ca and Mg to be accounted for by the reported dust deposition flux of 5-10 t km^{-2} y^{-1}, Ca and Mg concentration in dust would have to be in the range 1600-3200 and 800-1600 ppm, respectively. Such Ca and Mg concentrations are likely to be encountered in carbonate- and silicate-rich dust from global or regional emissions.

Regardless of the process leading to this enrichment of Ca, Mg, Al, Ti and Si in the Hakgala top soil, the added carbonate and silicate minerals will dissolve to varying degrees and will contribute to the dissolved load present in rivers. These non-denudational inputs have to be corrected for when estimating weathering rates in the rivers from the Sri Lankan Highlands.

4.4. Implications for stream chemistry and watershed denudation rates

4.4.1 Identifying weathering end members from inversion of small stream chemistry data

The chemical composition of soil pore water and of small creeks around Hakgala is plotted in the Mg/Na-Ca/Na space in Figure 8A. These element ratios are not sensitive to dilution by water. The composition of deep pore water close to the weathering front, calculated using equation 8, is also plotted. Soil pore water is enriched in both Ca and Mg as compared to the computed deep pore water. Published chemical compositions of carbonate rocks in Sri Lanka (Pitawala et al., 2003) and rock phosphate fertilizer (Dahanayake, 1995) allow positioning of these end members in Figure 8B. Local rainwater has average Mg/Na = 0.6 and Ca/Na = 1.5 (Silva and Manuweera 2004), but as uncertainties of these estimates are high, the data is not shown in Figure 8. Assuming congruent weathering of carbonate material, the soil water data is consistent with the dissolution of carbonate in the top soil (Figure 8). The significant spatial variability of the top soil water composition is most likely due to different water pathways and residence time in top soil between samples.

The chemical composition of the small creeks plot well within the array defined by the two pore water pools.The significant spatial and temporal variability in the small creeks' chemical composition most

likely derives from the spatial variability in topsoil porewater composition. However, regardless of the pathway of pore water to river water, the small creeks' dissolved load is ultimately derived from three sources: (1) rainwater; (2) weathering of Ca- and Mg-rich material in top soil, from hereon called the "top soil carbonate" end member; and (3) silicate weathering as occurring within the Hakgala regolith profile. In order to calculate the silicate weathering rate at the small creeks' scale, the other contributions have to be corrected for. The element ratios of the small creeks' dissolved load can be described with the following mixing equation:

$$\left(\frac{X}{Mg}\right)_{creeks} = \sum_i \alpha_i(Mg) \cdot \left(\frac{X}{Mg}\right)_i \qquad (13),$$

with i standing for each end member (rainwater, top soil carbonate, and silicate weathering), $\alpha_i(Mg)$ the contribution of end member i to the Mg carried by the small creeks' dissolved load, and X = Na, Ca, K, and Si. We assume that uptake of X by biota is balanced by biomass decay, such that the contribution of biological activity is ignored in equation (13). In contrast to what is done in many studies using Na as the normalizing element in equation (13), Mg is used here because the carbonate end member does not contain significant amounts of Na, K, or Si. However, Mg can be replaced by Ca in equation (13). Although the main unknowns of equation (13) are the $\alpha_i(Mg)$, there is some uncertainty associated with the chemical ratios of the creeks, which vary between individual creeks and are also not uniform with sampling time for a given creek (Table S2). Considerable uncertainty is also associated with the element ratios of the end members. Such *a priori* uncertainties can be taken into account when solving equation (13) through a full inversion procedure as used by Négrel et al. (1993) and Gaillardet et al. (1999b).This inversion procedure aims to provide a likely solution to the budget equations (eq. 13) in a least-squares sense, by iteratively adjusting the values of the different parameters (element ratios and contributions from each end member) within the constraint given by the *a priori* values on these parameters and the associated uncertainties. The values calculated thereby and the resulting associated uncertainties are the *a posteriori* parameters.

In addition to the elemental concentrations measured in samples and associated errors, the inversion method requires estimates for both the values and uncertainties for the chemical composition of end members, as well as for the contribution of each end member to rivers as *a priori* inputs. The silicate end member X/Mg ratios can be estimated using eq. 8 with the τ-values measured at the top of the Hakgala saprolite, which integrate the entire silicate weathering sequence in the weathering profile, while not being affected by addition from external sources. Values are shown in Table 9. The top soil carbonate end member is assumed to contain no significant Si, K, or Na, and to have a Ca/Mg mass ratio of 2.0 ±1.0(ratio of topsoil, see section 4.3) assuming congruent weathering. We therefore ignore weathering of any dust-derived silicate material in top soil. For the rainwater end member, data reported by Silva and Manuweera (2004) on rainwater chemistry in the Sri Lankan Highlands is used (Table 9). The X/Mg ratios of the mixture, *i.e.* the river water, are calculated from the average of the three creeks taken during three sampling campaigns excluding the HAK-2011-S3-3 sample that is potentially affected by domestic waste of fertilizer inputs (Section 3.7, Table S2).

The inversion yields that silicate weathering, topsoil carbonate dissolution, and rainwater contribute to the Mg budget in the three small creeks to ca. 17%, 60% and 23%, respectively. The same type of inversion using X/Ca ratios indicates that these contributions are 28%, 49% and 23% for Ca, respectively (Table 9). From these relative contributions and the composition of the end members, it can be inferred that ca. 55% of Na and 78% of K is derived from silicate weathering, the rest being supplied by rainwater. All Si is derived from silicate weathering, by definition. Summing up these contributions, it appears that 84% of the cationic load (calculated here as Na+Ca+K+Mg+SiO_2) of the Hakgala small creeks is derived from silicate weathering reactions.

The next step is to use these end member contributions with discharge data to compute weathering fluxes. However, the runoff of the small creeks is not known. In the following section, we instead estimate weathering rates from river dissolved loads of the large, gauged catchments in the Sri Lankan Highlands. Since both atmospheric inputs and top soil carbonate weathering contribute significantly to the small creeks dissolved load, such contributions have to be corrected for when evaluating silicate weathering rates at the larger catchment scale.

4.4.2Large catchment river chemistry

The solute loads of large monitored catchments in the Sri Lankan Highlands (von Blanckenburg et al., 2004) reflect mixing between the same end members as those identified in the small creeks (Figure 8B). However, the array defined by the large catchments covers much higher Ca/Na (around 4.5 times) and Mg/Na (around 3 times) than that covered by small creeks. For most rivers, this difference can be explained by the addition of carbonate material releasing Ca and Mg to the large rivers to a larger extent than that is observed at the small creeks' scale (Figure 8B). The most likely explanation for this feature is the significant presence of agricultural land (hence the intensive use of carbonate rocks as fertilizers) in the large river catchments, but might also be due to a larger lithologic fraction of marble bands at this scale. In addition, for the Huluganga (HUG) and Peradenyia (M-PER) rivers, a contribution of a third end member, with lower Ca/Mg ratio than carbonates, is necessary to explain the data. This end member is likely to be rock phosphate (Figure 8B). Here we consider only those 5 rivers (AO, BO, MO, NO, UO) for which the chemical composition can be explained by a binary mixture between (a) dissolved species derived from small, pristine creeks like those we sampled near Hakgala (see previous section) (b) dissolved species from the dissolution of carbonate material, be it marble bands present in bedrock or carbonate fertilizers. Given the trend formed by the data points associated with these rivers in Figure 8B, the most likely composition for the Ca- and Mg-rich end member at the scale of these large catchments is around Ca/Na = 1000 and Mg/Na = 100. Note that the Ca/Mg ratio of this carbonate end member, similar to that reported for carbonate rock in Sri Lanka (Pitawala et al., 2003) is much higher than that of the top soil carbonate end member identified at the regolith and small creeks' scale (section 4.4.1). Therefore, we refer in the following to this carbonate end member at the large catchment scale as the "Sri Lankan carbonate" end member. Using the Ca/Na and Mg/Na ratios in a binary mixture model, it can be shown that less than 1% of the dissolved Na in the large catchments is derived from carbonates. Hence the 2.2- to 5.2-fold increase in the Ca/Na ratio between small creeks and large rivers corresponds to an equivalent increase in the Ca flux, meaning that between 54 and 85% of dissolved Ca in large rivers is derived from Sri Lankan carbonates, depending on the river. The rest is derived from small creeks such as those we sampled near the Hakgala regolith profile. With a similar calculation, it can be shown that the Sri Lankan carbonate end member contributes to between 44 and 72% to the Mg load of large rivers in the central Highlands of Sri Lanka.

Combined with the cationic yields estimated in Table S2 (section 3.7) and the contribution of silicate weathering to each dissolved species in small creeks (section 4.4.1), it can be estimated that silicate rocks in the Sri Lankan Highlands are weathering at a rate of 18-36 t $km^{-2}y^{-1}$, or between 6and 13 mm ky^{-1}, assuming a rock density of 2700kg m^{-3} (Table 7). These numbers overlap with the calculations made previously (von Blanckenburg et al., 2004) using a different correction method, for the Uma Oya and the other catchments in the Upper Mahaweli Watershed.

4.5 Soil production, weathering, and erosion in the Sri Lankan Highlands: rates and controls

4.5.1 Long-term steady-state denudation

While denudation rates from cosmogenic nuclides average at 42 t km^{-2} y^{-1} or 15.5 mm ky^{-1} when corrected for mass loss between the depth of cosmogenic nuclide production (Table 7), a rate of ca. 5 mm

ky^{-1} is calculated for the propagation of the weathering front from the K-feldspar depletion profile (section 4.2). Combining the denudation rate with CDF, a weathering rate of 22 t km^{-2} y^{-1} or 8 mm ky^{-1}, averaged over 10^4 y, can be calculated. This number is in agreement with the silicate-derived oxide weathering rates calculated from river dissolved loads, averaging over <10 y, which are 18-36 t km^{-2} y^{-1}, corresponding to 6-13 mm ky^{-1} (Table 7; section 4.4.2). This similarity in denudation and weathering rates between these different methods and over the two time scales at 10 y and 10^4 y suggest a long-term steady state of denudation, meaning that saprolite production is balanced by export of material from the regolith by weathering and erosion.

4.5.2 Soil production rates in the Sri Lankan Highlands compared to other settings

After correction for saprolite dissolution, the denudation rate D_{corr} in Sri Lanka (interpreted here as a saprolite production rate) of 42 t km^{-2} y^{-1} inferred from cosmogenic nuclides (Table 7) can be compared to other tropical saprolite production rates. These are all restricted to a low range: 5 t km^{-2} y^{-1} in the Nsimi (Cameroon) catchment (Braun et al., 2012), 60 t km^{-2} y^{-1} in the south Indian Mule Hole catchment (Braun et al., 2009), and 20 t km^{-2} y^{-1} for laterite formed over gneiss in Cameroon (Dequincey et al., 1999). In support of these low saprolite production rates, the pioneering study of Edmond et al. (1995) on the mountains of the South-American Guyana Shield also resulted in similarly low weathering rates. These rates differ substantially from those found in tectonically active tropical settings: in the Luquillo granodiorite (Puerto Rico) estimates for saprolite production rates range from 90 t km^{-2} y^{-1} (Riebe et al., 2003) to 200 t km^{-2} y^{-1} (summarised in Chabaux et al., 2013). The East African Rwenzori Mountains, formed by rifting, yield catchment-wide rates of 20 to 340 t km^{-2} y^{-1} (Roller et al., 2012). Therefore, the Sri Lankan Highlands display soil production rates typical of tectonically stable tropical areas underlain by crystalline rocks.

In a broader scope, we now compare the Sri Lanka soil production rates to a global compilation of soil production rates (Figure 9; Dixon and von Blanckenburg, 2012). Here, measured denudation rates $D_{measured}$ are directly used to allow the comparison with other studies and are interpreted as soil production rates. Sri Lanka soil production rates plot at the lower end of the array, and are with 28t km^{-2} y^{-1} (here uncorrected for saprolite dissolution) distinctly lower than the global median soil production rate of 70 t km^{-2} y^{-1} (Dixon and von Blanckenburg, 2012). Only at Point Reyes, California (Burke et al, 2007) and in the Australian escarpment (Burke et al., 2009) are similarly low soil production rates found. Weathering rates from Sri Lanka (uncorrected for saprolite dissolution to allow for the comparison) are also at the lower end of the spectrum with 13 t km^{-2} y^{-1}, as compared to the global median for felsic soils of 20 t km^{-2} y^{-1} (Dixon and von Blanckenburg, 2012). This comparison shows that regolith renewal in Sri Lankan Highlands is slow as compared to the world average. The present detailed documentation of weathering and erosion rates in such a slow setting allows us in the following to discuss the relationship between erosion and weathering for one of the end members to recognised global relationships (Riebe et al., 2004;West et al., 2005, Dixon et al., 2009b; Norton et al., 2010; Dixon and von Blanckenburg, 2012).

4.5.3 Supply-limited weathering regime

The low weathering rates suggest that the denudation regime in this region is supply-limited (Riebe et al., 2004). This finding is supported by CDF values calculated for bedrock to soil conversion that have reached the maximum limit of 50% of the total denudation, as shown by the position on the CDF = 0.5 - line of the Sri Lanka data in Figure 9. Indeed, the charnockite contains 30% quartz (Table 1) that weathers very slowly (Schulz and White, 1999) and 20% Al_2O_3 + Fe_2O_3 (Table 3) that remain in the solid weathering residue, as inferred from τ-plots (Figure 6). Accordingly, XRD data show that the upper saprolite is mainly composed of primary quartz and secondary clay products (Table 2). As no weatherable mineral is present in the upper saprolite at Hakgala, the only way to increase the long-term weathering flux out of the profile would be to increase the supply of fresh mineral at the bottom of the regolith. In the

following we review the different reasons that could explain why this supply is low in Sri Lankan Highlands.

4.5.4 Potential factors controlling weathering

In the Sri Lankan Highlands, the slow advance of the weathering front, or in other words, the low saprolite production rate, is balanced by (1) slow weathering occurring throughout the regolith and (2) slow erosion of loose material from top soil. We now explore the potential reasons why this process is slow in the Sri Lankan Highlands.

A first possible explanation is that lithology controls the slow advance of the weathering front. Gunnell and Louchet (2000) have argued that the Sri Lankan and South Indian charnockite is particularly resistant to weathering. They based their conclusion on 1) the observation that charnockite always forms the ridges of highest relief, hence that the landscape is lowering divergently with charnockite weathering slowest; and 2) that permeability of charnockite rock as identified by soluchrome tests and mercury porosimetry is exceedingly low, hence water does not percolate easily into this rock. A full evaluation of this hypothesis is beyond the scope of this paper. We suspect, however, that non-charnockitic felsic lithologies, such as various types of gneiss, weather at similarly low rates as we observe at the Hakgala charnockite location. First, the cosmogenic nuclide- and mass balance-derived weathering rates of 21 t $km^{-2}y^{-1}$ determined at the Hakgala charnockite site are within error identical to the dissolved silicate-derived weathering yield (16-34 t $km^{-2}y^{-1}$, corrected for mass loss beneath the cosmic ray attenuation path length) measured on 5 large streams draining the Sri Lankan Highlands (Table 7). Yet in the Highlands and at the Hakgala site, charnockite is intercalated intimately with other metamorphic lithologies such as marble, quartzite, calc-gneiss, quartzofeldspathic gneiss and garnet-sillimanite-biotite gneiss (Figure 1B), and charnockitic rocks cover only about 50% of the Highland area. Hence, as the area of more "common" gneiss is so high, its weathering rate should be equally low. Second, a similar argument can be made for the cosmogenic nuclide data on river basins from the Highlands. Denudation rates (including physical erosion) from small forested catchments are similarly low at 5 to 30 t km^{-2} y^{-1} (von Blanckenburg et al., 2004). Some large rivers from the Highland yield higher rates (up to ca. 100 t km^{-2} y^{-1}, von Blanckenburg et al, 2004). We cannot exclude that these elevated rates reflect the predominance of faster weathering lithologies in these catchments. However, von Blanckenburg et al. (2004) discussed that these high rates might only be apparent if they result from dissection of the landscape by land use-related erosion. Another cause might be that these large rivers capture the geomorphic expression of escarpment retreat, documented by even higher rates (Vanacker et al. 2007a). In both cases, the cause for the increased cosmogenic nuclide derived denudation rates of the large catchments is geomorphic, not lithologic.

A second set of explanation, revolving around the hydrological properties of deep saprolites in tropical areas, was suggested by Edmond et al. (1995) for the Guyana Shield. There, the low rates of weathering were attributed to a combination of 1) impervious clay-rich regolith layers limiting the local flux of water to the weathering front; 2) the strong seasonality of precipitation limiting the exposure of the mineral surfaces at depth to water only during a fraction of the hydrological cycle; and 3) the low hydraulic gradient of the weathering front resulting in low water fluxes out the weathering profiles. In this way, thicker regoliths would result in a slower weathering front. This hypothesis could be supported if an inverse relationship between regolith thickness and production rates was observed (as modeled by Lebedeva et al., 2011), similar to the soil production function (Heimsath et al., 1997). However, in the few settings where both estimates of regolith thickness and weathering advance rates exist (see section 4.5.1) no such correlation is apparent, as mean approximate regolith thickness is 9 m for the Cameroon laterite (Dequincey et al., 1999), 17m in Mule Hole (Braun et al. 2009), 22 m in Nsimi (Braun et al., 2012), 7 m in Luquillo (Buss et al., 2008), 12m in Hakgala, Sri Lanka, and in any case even at a single location saprolite thickness is mostly highly variable and the lower boundary poorly defined.

It could also be argued that low erosion rates themselves slow the advance of the weathering front at depth. This would first require that the erosion rate signal at the surface is transmitted to the weathering front at depth through a feedback mechanism. As explained above, low erosion rates might promote regolith thickening and result in hydrological conditions at the weathering front that are unfavourable to weathering front advance (Edmond et al, 1995). In addition, the various models suggested for the weathering front advance help to evaluate this hypothesis. Of these models, only that of Fletcher et al. (2006) for spheroidal weathering offers an explicit feedback between erosion at the surface and weathering at depth. In this feedback, slow erosion would promote formation of deeper regolith and thereby limit oxygen transport to the weathering front. The ensuing lack of oxygen supply hinders further iron oxidation, resulting in a lack of positive volume strain and rock fracturing. Similar feedbacks are conceivable in other models of weathering front advance, but have not yet been explored. For example, hierarchical fracturing aided by volume expansion when secondary minerals precipitate in pores (Røyne et al., 2008; Jamtveit et al., 2009; Jamtveit et al., 2011), also suggests that the penetration of water and protons to depth is a function of regolith thickness and erosion, as it is in the Fletcher et al. (2006) model. Similarly, the opening of porosity during weathering rind formation and plagioclase dissolution should be able to promote access of fluids to unweathered rock (Sak et al., 2010; Navarre-Sitchler, 2011). This process is also dependent on proton supply at depth in the regolith. Finally, we can envisage a similar feedback if saprolite production is controlled by the utilization of mesofractures by fungal hyphae to supply water and mineral-dissolving reagents (Graham et al., 2010, Brantley et al, 2011).

Concerning the oxidation model, we note that although the charnockite bedrock of the Sri Lankan Highlands contains biotite, the first mineral to weather is pyroxene, followed closely by plagioclase. Biotite, in contrast, remains relatively stable during corestone weathering. If the creation of microfractures by oxidative volume increase (Fletcher et al., 2006; Lebedeva et al., 2007) is at all a mechanism that enables a feedback, then it takes place through orthopyroxene alteration. Intense plagioclase conversion to secondary products observed in the Hakgala corestone is in turn likely to be the process converting cohesive material (such as observed in zone 3) into disaggregated rinds (zone 4) that surrounds the corestones and eventually forms saprolite.

The hypothesis of low erosion rates controlling the slow advance of the weathering front in Sri Lanka also requires an explanation for the low erosion rates. A possibility is that the thick forest canopy limits erosion. We know that vegetation cover potentially decreases hillslope erosion rates (Istanbulluoglu and Bras, 2005; Vanacker et al., 2007b). In this regard it is important to note that the Sri Lankan Highlands were covered with a thick tropical forest until the onset of intense land use 300 years ago, and that its removal led to a strong increase in erosion rate (Hewawasam et al., 2003). The Hakgala site presented in this study is still covered with a thick, natural rain forest. However, presently we know too little about these ecological controls to evaluate this possibility.

Therefore, the tectonic quiescence hypothesis (von Blanckenburg et al., 2004) is still the most likely explanation for both slow erosion and slow advance of the weathering front. Concerning the processes at the weathering front, igneous rocks that were not recently deformed and faulted are less susceptible to access by the fluids required for advancing the weathering front at depth. This absence of deformation might be the case for the exhumed Proterozoic rocks comprising the Sri Lankan Highlands that may have even never been deformed intensively in the brittle regime and thereby not offer preferential access to rock surface for fluids (Molnar et al., 2007). However, we note that, for the crystalline basement of Sri Lanka, several episodes of brittle deformation have been inferred for the Cretaceous period based on thermochronological data (Emmel et al., 2012). Concerning the erosion rate, the lack of active faulting leads to constant stream base level and comparatively stationary subsurface hydrologic pathways. Therefore, tectonic quiescence favors slow weathering at depth in regolith and inhibits erosion processes from hillslopes. The distinctly higher soil production rates found in tectonically active tropical areas lend support to this hypothesis.

5. Conclusions

We explored the chemical and mineralogical transformations taking place during weathering in a 10 m deep tropical regolith profile. We used three independent means to calculate rates of weathering: 1) cosmogenic nuclides and chemical depletion fractions (CDF) were used to determine the profiles' local weathering rates; 2) the regional spatially averaged landscape weathering flux was determined from a combination of the chemical composition of pristine creeks draining a natural reserve and discharge data from gauging of large rivers from within the Upper Mahaweli catchment; and 3) the advance rate of the saprolite weathering front was calculated from element and mineral concentration gradients.

Rates from 1) and 2) agree at 16 to 36 t km^{-2} y^{-1}, corresponding to a weathering front advance rate of 6-13 mm ky^{-1}. Method 3) also falls within this range, despite the high systematic uncertainties associated with the calculation of the advance rate. Given this agreement, we consider the weathering system to be operating at steady state over the 10^1 to 10^4 year time scale, which are the integration times of the methods used.

The chemical depletion fraction reaches an average value of 50% at the top of the profile, and primary quartz and secondary clays and oxides are the only minerals left. This means that the weathering system is firmly within the supply-limited regime.

The processes at the weathering front manifest themselves in the form of corestones of all sizes that form clay and oxide-rich rinds around charnockite bedrock. The rinds allow reconstruction of the sequence of mineral decomposition which is pyroxene; plagioclase; biotite; K-feldspar. Since biotite is not the first mineral to weather in the corestone, the proposed oxidation mechanism to advance the weathering front(Fletcher et al., 2006; Lebedeva et al., 2007; Buss et al., 2008)can only rely on pyroxene oxidation. Alternatively, the observable changes in plagioclase and clay content suggest that processes involving positive volume change by clay formation (Røyne et al., 2008; Jamtveit et al., 2011) constitute a potential mechanism. In addition, the role of creation of secondary porosity by plagioclase dissolution (Sak et al., 2010; Navarre-Sitchler et al., 2011) or a biological feedback mechanism involving microbial rock decomposition at depth (Graham et al., 2010; Brantley et al., 2011) cannot be excluded at this stage.

Mineral decomposition occurs throughout the saprolite profile and only pyroxene and plagioclase are fully depleted at its base, resulting in quantitative loss of Ca and Na throughout the saprolite as seen by τ profiles. The top of the profile, comprising the organic-rich soil layer, is enriched in Mg, Ca, Rb, Fe, and Ti and non-radiogenic Sr when compared to the saprolite beneath it. The most likely cause is the entrainment of wind-blown (local or far-reaching aeolian) material rich in carbonate minerals. A full inversion of the small creeks' chemical composition shows that ca. 15% of the dissolved load is derived from rain and from the weathering of this wind-blown material.A non-silicate weathering contribution from dust sources, local marble bands and rain, amounts to 50% in the local pristine rivers. The remainder is supplied by weathering occurring throughout regolith.

The low denudation rate of the regolith of 15.5 mm ky^{-1} (when corrected for weathering mass loss beneath the cosmogenic nuclide attenuation depth), and the low weathering rates of 6-13 mm ky^{-1} are typical of tectonically quiescent tropical areas (*e.g.*Edmond et al., 1995). We speculate that these low rates are the result of high rock hardness, stagnant hydrological regime in deep regolith, or low erosion rates in a landscape devoid of geomorphic rejuvenation in prolonged periods of tectonic quiesence (von Blanckenburg et al., 2004). The weathering process taking place in the Sri Lankan Highland provides an exceptional end member case for slow, tropical, supply-limited weathering.

Acknowledgements. We thank R. Naumann and A. Gottsche for their help with XRF, XRD, and IC analyses. I. Schäpan is thanked for assistance during electron microscopy analyses. E. Lewin is

acknowledged for having provided the inversion software. T.H. was supported by the German Academic Exchange Service (DAAD) during his stay at GFZ Potsdam. We are grateful for the thorough and constructive reviews by three anonymous reviewers and the associate editor.

Figure Captions

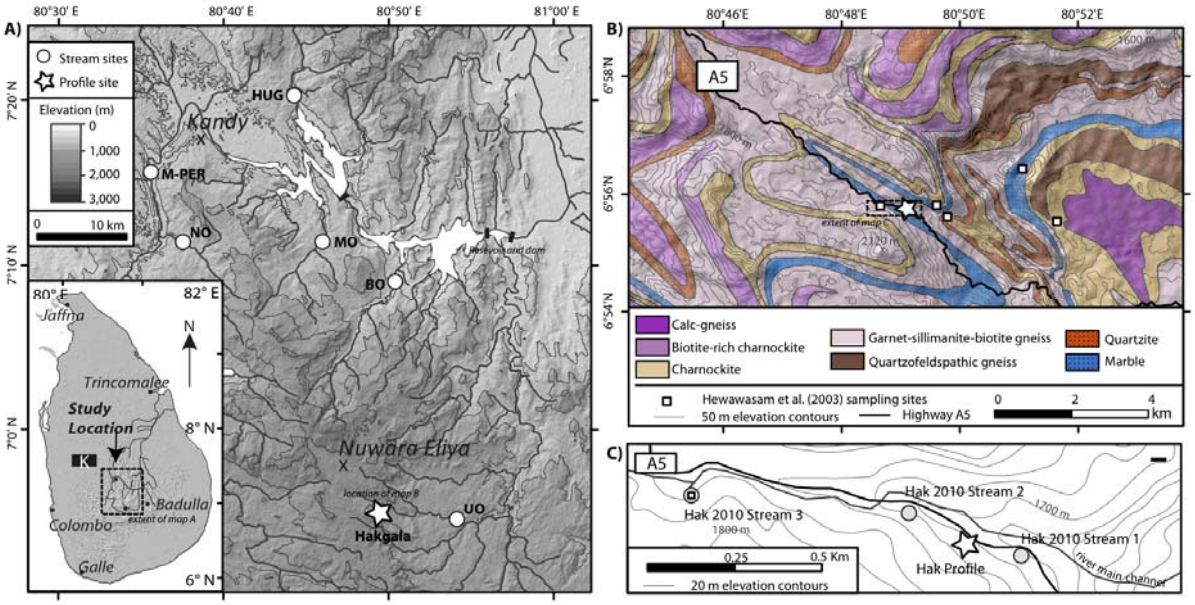

Figure 1 (A) Topographic map showing the locations of the small forested catchment at Hakgala (white star) and of the river gauging stations monitored for dissolved loads of the Upper Mahaweli catchment (white circles). Inset shows a map of Sri Lanka indicating the study area and the Kurunegala region (K, Burton and O'Nions, 1990). **(B)** Geologic map of the study area (Hakgala forested catchment) showing the underlying lithology, location of the regolith section (star) and of the small creeks (squares) sampled by Hewawasam et al. (2003) for cosmogenic nuclide analyses on sediment. Source: Geological Survey and Mines Bureau, Sri Lanka. Note that rock types are intercalated at still smaller scale than can be represented on this map. Hence our profile is nominally located over garnet-sillimanite-biotite gneiss, even though the local rock is charnockite. **(C)** Close up of B showing the location of the regolith section (star) and of the small creeks sampled for dissolved loads in this study (circles).

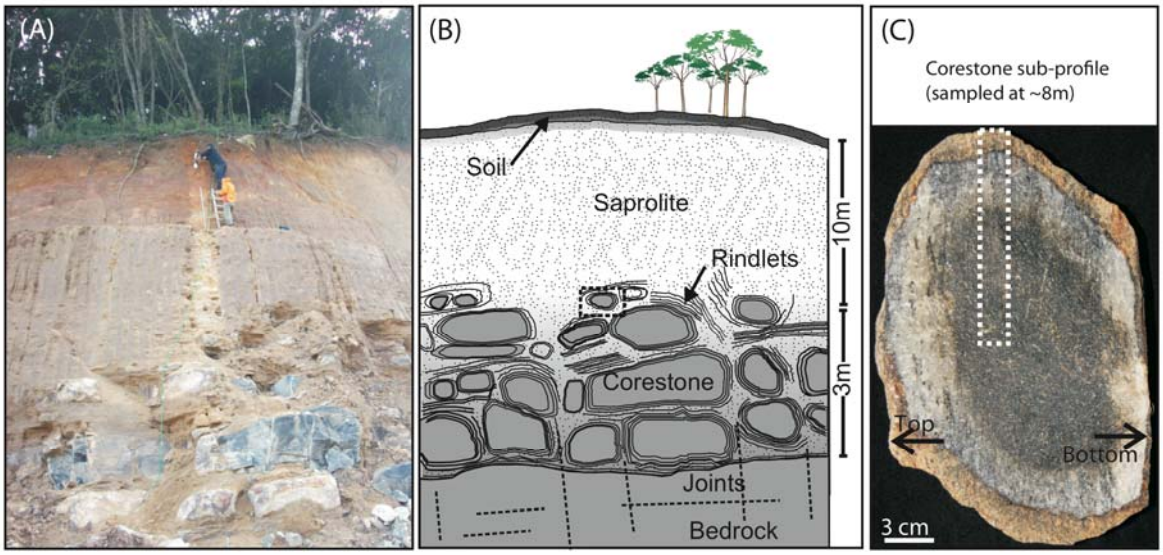

Figure 2 (A) Photograph and **(B)** simplified diagram showing the regolith profile developed at Hakgala (06.92923° N, 80.81834° E), exposed on a road cut from Nuwaraeliya to Welimada in the central Highlands of Sri Lanka. Note that corestones have been formed by initial weathering along the pre-existing joints and saprolite is formed from rinds that surround corestones developed by spheroidal weathering. Samples of soil and saprolite were collected from a vertical section. Nine bedrock samples were also collected from the underlying bedrock. **(C)** Photograph of the corestone sampled at 8.30 m depth (black dotted box in **(B)**) at Hakgala regolith profile. A slab of this corestone (white dotted box) together with two pieces of rinds surrounding the corestone (not shown in this photograph) were embedded in epoxy (Figure 3A) for mineralogical studies.

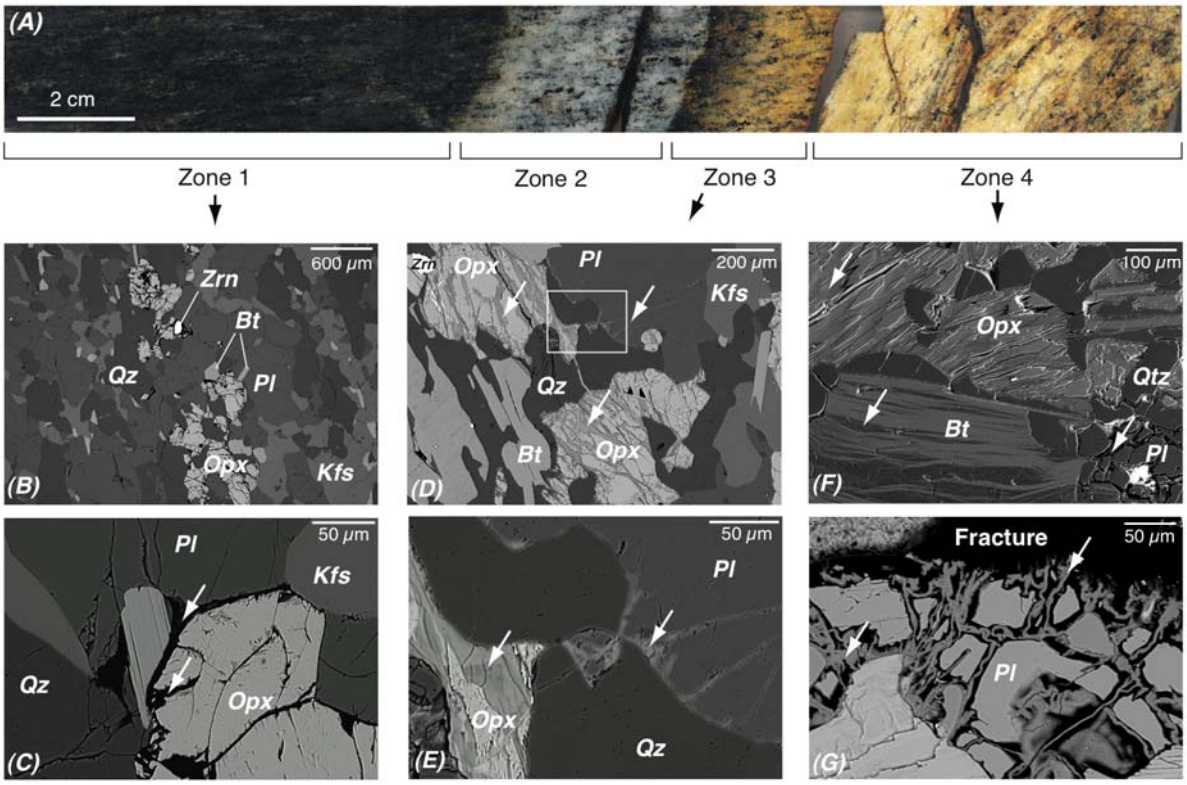

Figure 3 Electron-microscopic observations on the corestone sampled at 8.30 m-depth in the Hakgala weathering profile. Opx: orthopyroxene; Bt: biotite; Qtz: quartz; Pl: plagioclase; Kfs: K feldspar; Zrn: zircon; (A) Photograph of a 20 cm-long slab covering the whole radius of the corestone embedded in epoxy. The different zones, identified by optical inspection, are listed. (B) and (C): SEM (Backscattered electron (BSE)) images of zone 1 (unweathered core). Pyroxenes are highly fractured (white arrows in (C)), but other minerals show no significant weathering features. (D) and (E): BSE images of the bottom of the zone 3 (near the interface to zone 2). (E) is a close-up of (D) (white rectangle in (D)). Pyroxenes show alteration products as dark gray fillings of fractures (indicated by white arrows). This alteration feature was also observed in zones 2 to 4. Plagioclases appear light gray at the grain margins and in fractures (indicated by a white arrow), a feature that was observed only in zone 3. (F) Secondary electron (SE) images of the outer zone 4. Pyroxenes show ”low relief” (white arrow in the upper-left corner), while biotite is altered as shown by relatively dark layers intermingled with unweathered gray layers (white arrow in the lower-left corner). (G) BSE image of highly fractured plagioclases near a large void. Filamentous secondary material fills these fractures (white arrow; also visible near the white arrow in the lower-right corner of (F)).

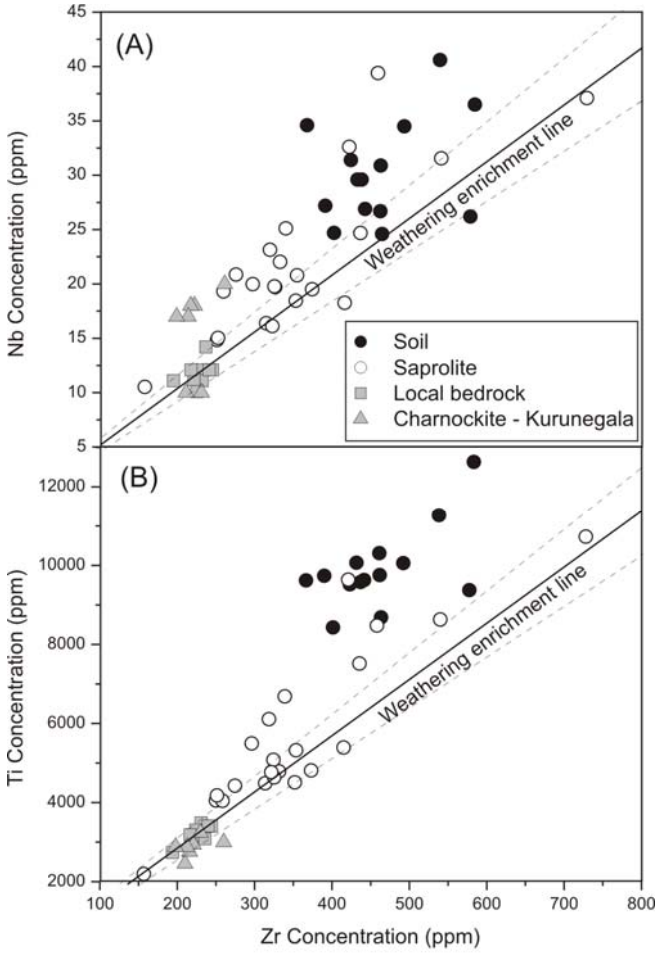

Figure 4

Figure 4 Immobile element concentrations measured in soil, saprolite and bedrock at the Hakgala regolith profile and for other charnockite rocks at Kurunegala (Hansen et al., 1987) in the Proterozoic terrain of Sri Lanka. The solid line (with error envelope) indicates the weathering enrichment line for bedrock composition, constructed from ratios of the initial element concentrations of the charnockite bedrock.

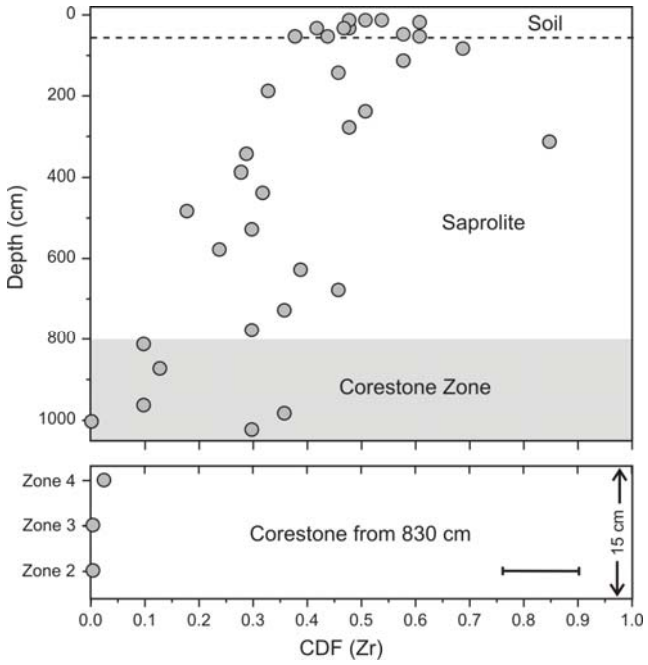

Figure 5 Chemical depletion fractions (CDF) based on Zr across the weathering profile showing an increase in the degree of weathering from bottom to the top in the saprolite profile (upper panel) and within a 15cm slab of the sampled corestone (lower panel). The grey area denotes the zone rich in partially weathered corestones (Fig. 2b). In this zone, the chemical depletion is highly variable depending on proximity of the saprolite sample taken to a partially weathered corestone. The CDF for bedrock to soil conversion is ca. 0.5 indicating that ca. 50% of the denudation is represented by chemical weathering in soil. Note that the CDF for bedrock to corestone formation is almost zero implying only minor mass loss has occurred during spheroidal weathering. Relative uncertainty in CDF values are about 14% (indicated by a representative error bar at the bottom-right).

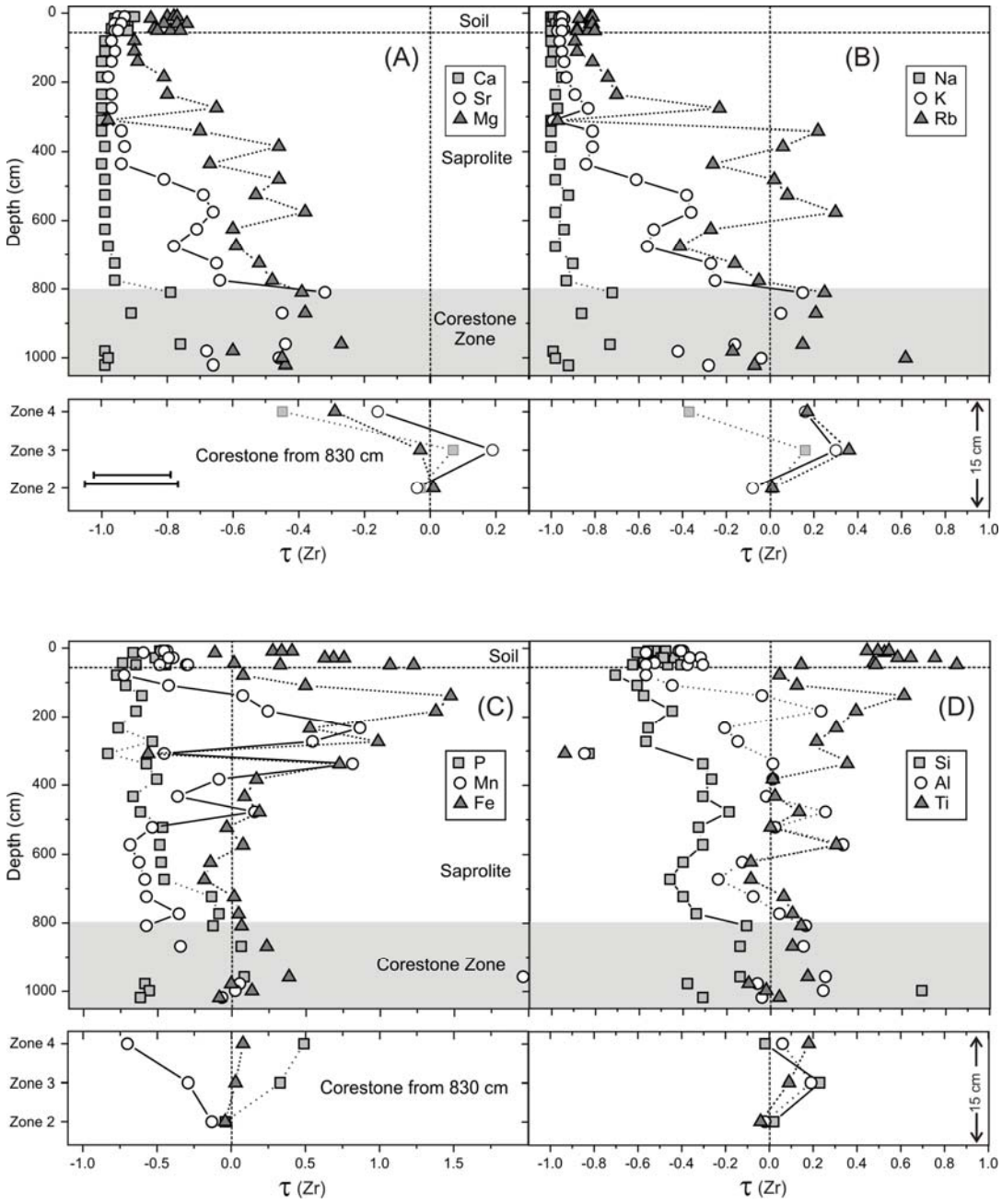

Figure 6 Elemental mass transfer coefficients (τ) versus depth for soil, saprolite (upper panels) and for 15cm slab from the sampled corestone (lower panels) of the Hakgala regolith profile. The grey area denotes the zone rich in partially weathered corestones (Fig. 2b). In this zone, τ values are highly variable depending on proximity of the saprolite sample taken to a partially weathered corestone. Note that the average elemental concentration of 9 bedrock samples was used as representative bedrock composition (Table 3). The sample of SL14 Hak 2010 (Table 4), which is unusually enriched in Zr (4 times greater than the average Zr concentration in saprolite), was considered as an outlier and excluded in plotting τ with depth. Based on uncertainties of XRF measurements, the relative uncertainties in τ values are estimated to be about 16% for major elements and about 20% for minor elements (indicated by representative error bars at the bottom-left of panel A).

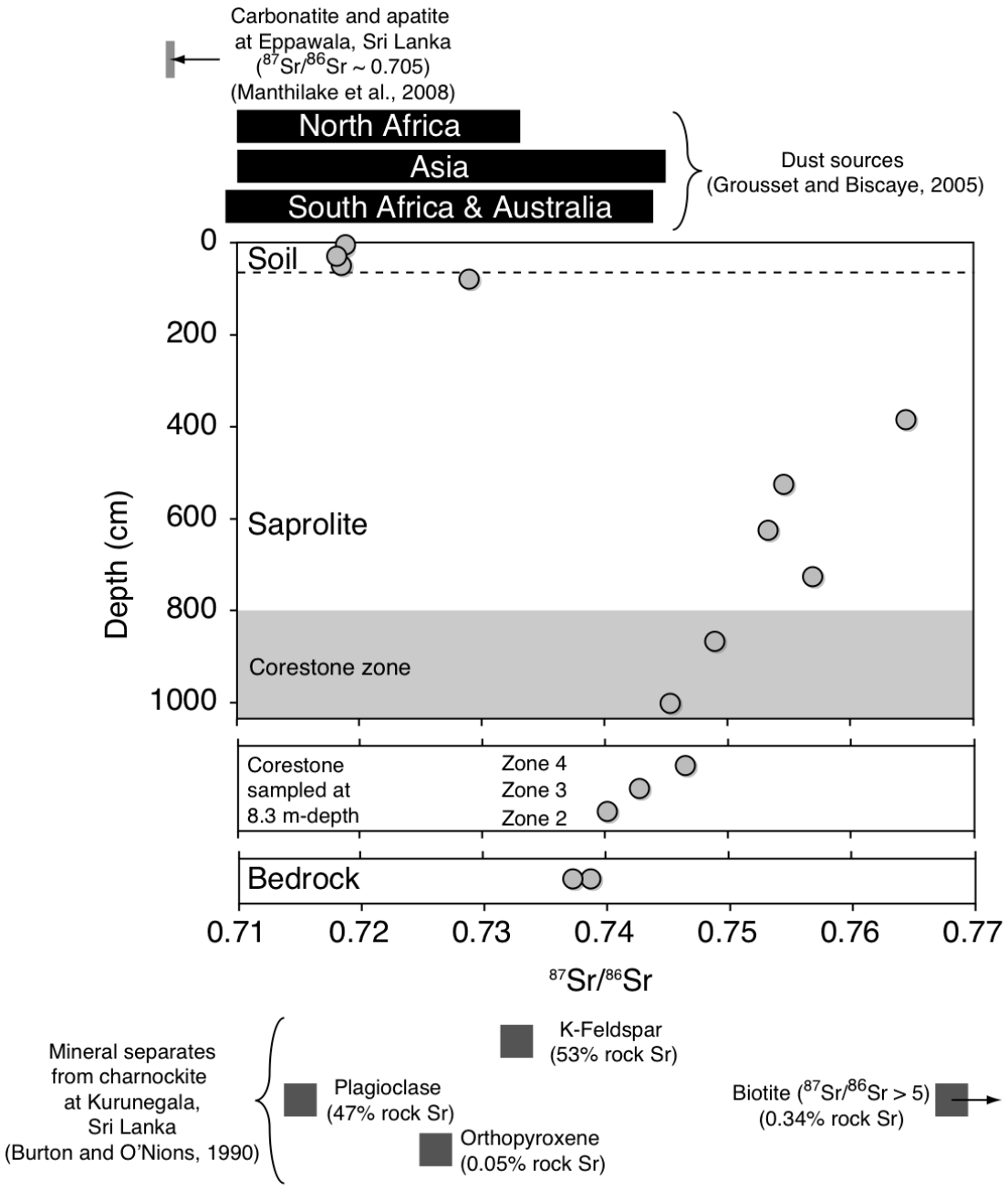

Figure 7 Sr isotope ratios ($^{87}Sr/^{86}Sr$) at the Hakgala weathering profile as a function of depth. Sr isotope ratios obtained for bulk bedrock and from the corestone sampled at 8.30 m depth are shown in the bottom panel (definition of the corestone zones are provided in the text and in Figure 3). Estimates of Sr isotope ratios in different dust sources (from Grousset and Biscaye, 2005) and of carbonatite which are potential apatite fertiliser sources (Manthilake et al, 2008) are shown at the top, and Sr isotope ratios reported by Burton and O'Nions (1990) for mineral separates from charnockite at Kurunegala, Sri Lanka, are shown at the bottom along with the percentage of rock Sr carried by each mineral type. Data and errors (smaller than symbols) are given in Table 5.

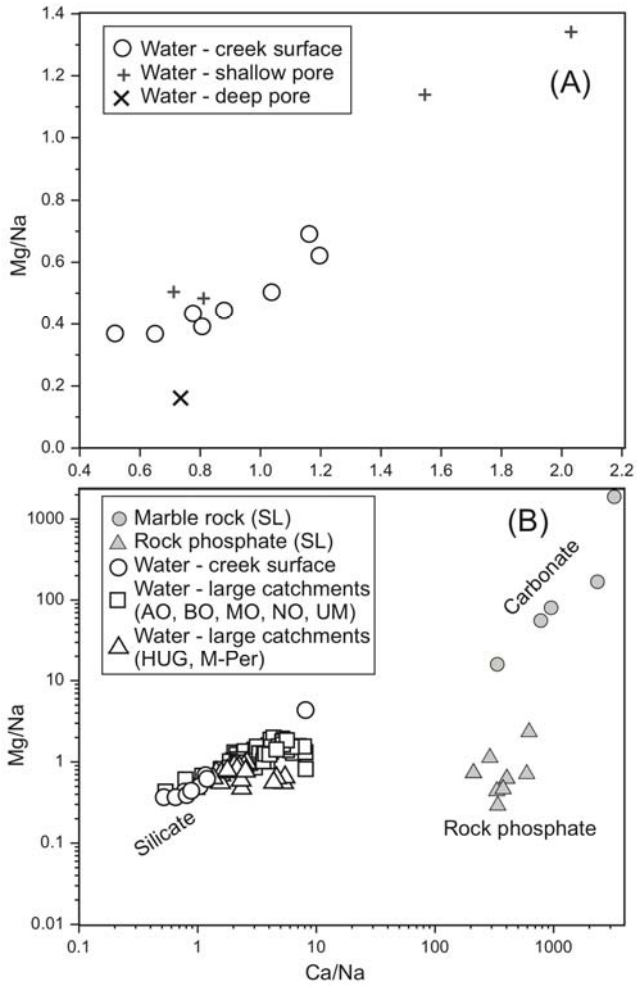

Figure 8 Plots of **(A)** Mixing trend between shallow and deep pore water composition in pristine creeks. Deep pore water elemental ratios were calculated from deep saprolite compositions based on -τ values (equation 7). **(B)**Mixing trend and end members of stream water for the monitored large rivers in the central Highlands of Sri Lanka. The silicate end member is defined from solute chemistry in pristine creeks drained on silicate lithologies, measured pore water chemistry in soil at the Hakgala regolith profile, and calculated pore water chemistry based on -τ values (equation 7). Carbonate and rock phosphate end members are defined from whole rock chemistry (Dahanayake, 1995; Pitawala et al., 2003) assuming that they weather congruently.

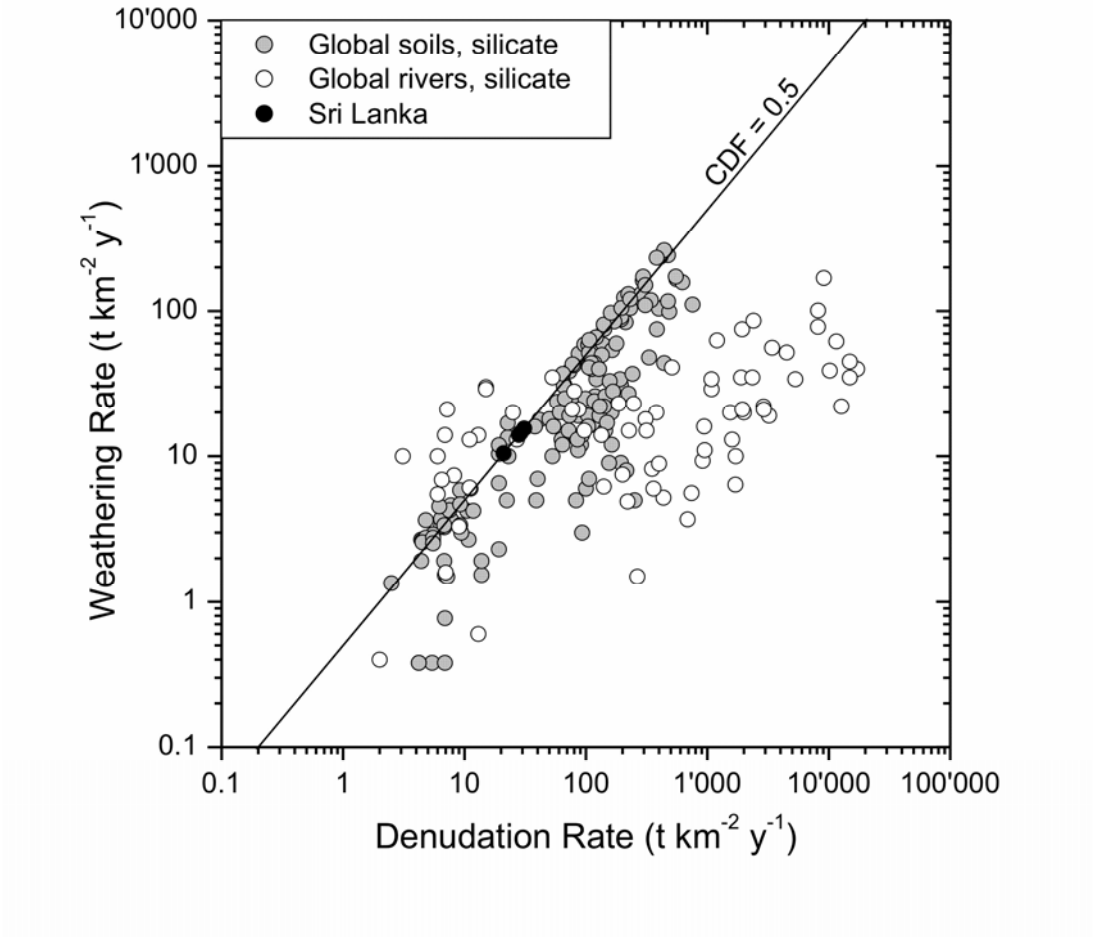

Figure 9 Denudation verses weathering rates from Hakgala soil and creek sediments (black) compared to globally distributed soil rates (grey) from cosmogenic nuclides and CDF on felsic lithologies and to global silicate denudation and weathering rates from river suspended and dissolved loads (open symbols). The global data sources are as compiled by Dixon & von Blanckenburg (2012). At steady state soil denudation rates also represent soil (or saprolite) production rates. The Hakgala data is composed of the two soil and two creek sediment denudation rates presented in Table 7 that were multiplied with the CDF of 0.5 measured for the soil in our profile to calculate weathering rates. Rates are presented without correction for saprolite dissolution (eq. 4) to allow for direct comparison with the other cosmogenic nuclide data that is also uncorrected. For reference the solid line denotes a CDF of 0.5 which is mostly the maximum chemical depletion attainable in granitoid lithologies. Data plotting on this line is in the "supply-limited" regime, whereas data plotting to the right of this line is from "kinetically limited" settings. Dissolved data plotting to the left of the line is most likely due to dissolved fluxes not being in balance with the associated suspended load fluxes. Sri Lanka soil production rates are in the lower range of the global data that is capped by a postulated upper limit of 320 to 450 t km^{-2} y^{-1}; Sri Lanka weathering rates are in the lower range of global soil and saprolite weathering rates that are capped by a postulated upper limit of 150 t km^{-2} y^{-1} (Dixon and von Blanckenburg, 2012).

References

Anderson, S.P., Dietrich, W.E., Brimhall, G.H., 2002. Weathering profiles, mass-balance analysis, and rates of solute loss : Linkages between weathering and erosion in a small, steep catchment. *Geol. Soc. America Bulletin* **114**, 1143-1158.

Braun, J.J., Marechal, J.C., Riotte, J., Boeglin, J.L., Bedimo, J.P.B., Ngoupayou, J.R.N., Nyeck, B.,Robain, H., Sekhar, M., Audry, S., Viers, J., 2012. Elemental weathering fluxes and saprolite production rate in a Central African lateritic terrain (Nsimi, South Cameroon). *Geochim.Cosmochim. Acta* **99**, 243-270.

Braun, J. J., Descloitres, M., Riotte, J., Fleury, S., Barbiero, L., Boeglin, J. L., Violette, A., Lacarce, E., Ruiz, L., Sekhar, M., Kumar, M. S. M., Subramanian, S., and Dupree, B., 2009. Regolith mass balance inferred from combined mineralogical, geochemical and geophysical studies: Mule Hole gneissic watershed, South India. Geochim.Cosmochim. Acta **73**, 935-961.

Blum, J. D. and Erel, Y., 1997. Rb-Sr isotope systematics of a granitic soil chronosequence: The importance of biotite weathering. *Geochim.Cosmochim. Acta* **61**, 3193-3204.

Brimhall, G., Dietrich, W.E., 1987. Constitutive mass balance relations between chemical composition, volume, density, porosity, and strain in metasomatic hydrochemical systems: results on weathering and pedogenisis. *Geochimca et Cosmochimica Acta* **51**, 567–587.

Brantley, S. L. and and 26 others, 2011. Twelve testable hypotheses on the geobiology of weathering.*Geobiology* DOI:10.1111/j.1472-4669.2010.00264.x.

Burke, B.C., Heimsath, A.M., Dixon, J.L., Chappell, J., Yoo, K., 2009. Weathering the escarpment:chemical and physical rates and processes, south-eastern Australia. *Earth Surface Processes and Landforms* **34**, 768-785.

Burke, B.C., Heimsath, A.M., White, A.F., 2007.Coupling chemical weathering with soil production across soil-mantled landscapes.*Earth Surface Processes and Landforms* **32**, 853-873.

Burton, K.W., O'Nions, R.K., 1990. The timescale and mechanism of granulite formation at Kurunegala, Sri Lanka. *Contribution to Mineralogy and Petrology* **106**, 66-89.

Buss, H.L., Sak, P.B., Webb, S.M., Brantley, S.L., 2008. Weathering of the Rio Blanco quartz diorite, Luquillo Mountains, Puerto Rico: Coupling oxidation, dissolution and fracturing. *Geochim. Cosmochim. Acta* **72**, 4488-4507.

Chabaux, F., Blaes, E., Stille, P., Roupert, R.D., Pelt, E., Dosseto, A., Ma, L., Buss, H.L., Brantley, S.L., 2013. Regolith formation rate from U-series nuclides: Implications from the study of a spheroidal weathering profile in the Rio Icacos watershed (Puerto Rico). *Geochim.Cosmochim. Acta* **100**, 73-95.

Chapman, R. W. and Greenfield, M. A., 1949.Spheroidal weathering of igneous rocks.*Am. J. Sci.* **247**, 407-429.

Cooray, P.G., 1994. The Precambrian of Sri Lanka: a historical review. *Precambrian Research* **66**, 3-18.

Cornu, S., Lucas, Y., Lebon, E., Ambrosi, J.P., Luizão, F., Rouiller, J., Bonnay, M., Neal, C., 1999. . Evidence of titanium mobility in soil profiles, Manaus, central Amazonia. *Geoderma* **91**, 281-295.

Dahanayake, K., 1995. Geological and geochemical aspects of Eppawala and Ridigama phosphate deposits of Sri Lanka, in: Dahanayake, K., Van Kauwenbergh, S.J., Hellums, D.T. (Eds.), Direct

application of phosphate rock and appropriate technology fertilizers in Asia - what hinders acceptance and growth. International Fertilizer Development Center Kandy, Sri Lanka, pp. 143-151.

Dahanayake, K., Ratnayake,M.P.K., Sunil, P.A., 1995. Potential of eppawala apatite as a directly applied low-cost fertilizer for rice production in Sri Lanka. *Fertilizer Research*, **41(2)**, 145-150.

Delattre, S.,Utsunomiya, S,Ewing, R.C.,Boeglin, J.L.,Braun, J.J., Balan, E.,Calas, G., 2007. Dissolution of radiation-damaged zircon in lateritic soils. *American Mineralogis,* **92**, 1978-1989.

Dequincey, O., Chabaux, F., Clauer, N., Liewig, N., Muller, J.P., 1999.Dating of weathering profiles by radioactive disequilibria: contribution of the study of authigenic mineral fractions. *Comptes Rendus de l Academie des Sciences* **328**, 679-685.

Dixon, J.L., Heimsath, A.M., Amundson, R., 2009a. The critical role of climate and saprolite weathering in landscape evolution. *Earth Surface Processes and Landforms* **34**, 1507–1521.

Dixon, J.N., Heimsath, A.M., Kaste, J., Amundson, R., 2009b. Climate-driven processes of hillslope weathering. *Geology* **37**, 975-978.

Dixon, J. L. and von Blanckenburg, F., 2012.Soils as pacemakers and limiters of global silicate weathering. *Comptes-RendusGeosciences* **344**, 597-609.

Dosseto, A., Buss, H.L., Suresh, P.O., 2012. Rapid regolith formation over volcanic bedrock and implications for landscape evolution.*Earth Planet. Sci. Lett.* **337**, 47-55.

Edmond, J.M., Palmer, M.R., Measures, C.I., Grant, B., Stallard, R.F., 1995. The fluvial geochemistry and denudation rate of the Guayana Shield in Venezuela, Colombia, and Brazil. *Geochim.Cosmochim.Acta* **59**, 3301-3325.

Emmel, B., F. Lisker, and T. Hewawasam, 2012. Thermochronological dating of brittle structures in basement rocks – acase study from the onshore passive margin of SW Sri Lanka, *J. Geophys. Res.*, doi:10.1029/2012JB009136.

Fletcher, R., Buss, H., Brantley, S., 2006. A spheroidal weathering model coupling porewater chemistry to soil thicknesses during steady-state denudation. *Earth Planet. Sci. Lett.* **244**, 444-457.

Fletcher, R. C. and Brantley, S. L., 2010. Reduction of bedrock blocks as corestones in the weathering profile: observations and model. *Amer. J. Sci.* **310**, 131-164.

Gaillardet, J., Dupré, B., Louvat, P., and Allègre, C. J., 1999a. Global silicate weathering and CO_2 consumption rates deduced from the chemistry of large rivers. *Chem.Geol.* **159**, 3-30.

Gaillardet, J., Dupré, B., Allègre, J.C., 1999b. Geochemistry of large river suspended sediments: silicate weathering of crustal recycling? *Geochim. Cosmochim.Acta* **63**, 4037-4051.

Godsey, S. E., Kirchner, J. W., and Clow, D. W., 2009. Concentration-discharge relationships reflect chemostatic characteristics of US catchments. *Hydrological Processes* **23**, 1844-1864.

Graham, R.C., Rossi, A.M., Hubbert, K.R., 2010. Rock to regolith conversion: Producing hospitable substrates for terrestrial ecosystems. *GSA Today* **20**, 4-9.

Grousset, F. E. and Biscaye, P. E., 2005. Tracing dust sources and transport patterns using Sr, Nd and Pb isotopes. *Chemical Geology* **222**, 149-167.

Gunnell, Y., Louchet, A., 2000. The influence of rock hardness and divergent weathering on the interpretation of apatite fission-track denudation rates. *Z. Geomorph. N. F.* **44**, 33-57.

Hansen, E.C., Janardhan, A.S., Newton, R.C., Prame, W.K.B.N., Kumar, G.R.R., 1987. Arrested charnockite formation in southern India and Sri Lanka. *Contrib.to Mineralogy and Petrology* **96**, 225-244.

Heimsath, A.M., Dietrich, W.E., Nishiizumi, K., Finkel, R.C., 1997. The soil production function and landscape equilibrium. *Nature* **388**, 358-361.

Hewawasam, T., von Blanckenburg, F., Schaller, M., Kubik, W., 2003. Increase of human over natural erosion rates in tropical highlands constrained by cosmogenic nuclides. *Geology* **31**, 597-600.

Istanbulluoglu, E. and Bras, R.L., 2005. Vegetation-modulated landscape evolution: Effects of vegetation on landscape processes, drainage density, and topography. *Journal of Geophysical Research-Earth Surface* **110**.

Jamtveit, B., Putnis, C., and Malthe-Sorenssen, A., 2009. Reaction induced fracturing during replacement processes. *Contributions to Mineralogy and Petrology* **157**, 127-133.

Jamtveit, B., Kobchenko, M., Austrheim, H., Malthe-Sorenssen, A., Royne, A., and Svensen, H., 2011.Porosity evolution and crystallization-driven fragmentation during weathering of andesite.*Journal of Geophysical Research-Solid Earth* **116**.

Jobbágy, E.G., Jackson, R.B., 2004. The uplift of soil nutrients by plants: biogeochemical consequences across scales. *Ecology* **85**, 2380-2389.

Kehelpannala, K.V.W., Wada, H., Ranaweera, L., Hamana, N., 2006. Cataclastic rocks from the granulite terrain of Sri Lanka: evidence for younger brittle deformation of the exhumed lower crust. *Geoscience Report, Shizuoka University* **33**, 9-19.

Kohfeld, K.E., Harrison, S.P., 2001. DIRTMAP: the geological record of dust. *Earth-Science Reviews* **54**, 81–114.

Lebedeva, M.I., Fletcher, R.C., Balashov, V.N., Brantley, S.L., 2007. A reactive diffusion model describing transformation of bedrock to saprolite. *Chem. Geology* **244**, 624–645.

Lebedeva, M.I., Fletcher, R.C., and Brantley, S.L., 2011. A mathematical model for steady-state regolith production at constant erosion rate. *Earth Surf. Proc. Landforms* **35**, 508-524.

Linton, D.L., 1955. The problem of tors. *The Geographical Journal* **121**, 470-487.

Ma, L., Chabaux, F., Pelt, E., Granet, M., Sak, P. B., Gaillardet, J., Lebedeva, M., and Brantley, S. L., 2012.The effect of curvature on weathering rind formation: Evidence from Uranium-series isotopes in basaltic andesite weathering clasts in Guadeloupe. *Geochim.Cosmochim. Acta* **80**, 92-107.

Manthilake, M.A.G.M., Sawada, Y., and Sakai, S., 2008, Genesis and evolution of Eppawala carbonatites, Sri Lanka. J. *Asian Earth Sci.* **32**, 66-75.

Mathieu, D., Bernat, M., Nahon, D., 1995.Short-lived U and Th isotope distribution in a tropical laterite derived from granite (Pitinga river basin, Amazonia, Brazil): application to assessment of weathering rate. *Earth Planet. Sci. Lett.***136**, 703-714.

Meybeck, M., 1987. Global chemical weathering of surficial rocks estimated from river dissolved loads. *Amer. J. Sci.* **287**, 401-428.

Milliman, J.D., Meade, R.H., 1983. World-wide delivery of river sediment to the oceans. *Journal of Geology* **91**, 1 - 21.

Molnar, P., Anderson, R.S., Anderson, S.P., 2007. Tectonics, fracturing of rock, and erosion. *J.Geophys.Res.* **112**, F03014.

Mulyanto, B., Stoops, G., Van Ranst, E., 1999. Precipitation and dissolution of gibbsite during weathering of andesitic boulders in humid tropical West Java, Indonesia. *Geoderma* **89**, 287-305.

Navarre-Sitchler, A. and Brantley, S., 2007.Basalt weathering across scales.*Earth Planet. Sci. Lett.* **261**, 321-334.

Navarre-Sitchler, A., Steefel, C. I., Sak, P. B., and Brantley, S. L., 2011.A reactive-transport model for weathering rind formation on basalt.*Geochim.Cosmochim. Acta* **75**, 7644-7667.

Negrel, P., Allegre, C. J., Dupré, B., and Lewin, E., 1993. Erosion sources determined by inversion of major and trace element ratios and strontium isotopic ratios in river water: The Congo Basin case. *Earth Planet. Sci. Lett.* **120**, 59-76.

Norton, K. P. and von Blanckenburg, F., 2010. Silicate weathering of soil-mantled slopes in an active Alpine landscape. *Geochim. Cosmochim. Acta* **74**, 5243-5258.

Ollier, C.D., 1971. Causes of spheroidal weathering. *Earth Sci. Rev.* **7**, 127–141.

Pitawala, A.H., Schidlowski, M., Dahanayake, K., Hofmeister, W., 2003. Geochemical and petrological characteristics of Eppawala phosphate deposits, Sri Lanka. *Mineralium Deposita* **38**, 505-515.

Prame, W.K.B.N., Pohl, J., 1994. Geochemistry of pelitic and psammopelitic Precambrian metasediments from southwestern Sri Lanka: implications for two contrasting source-terrains and tectonic settings. *Precambrian Research* **66**, 223-244.

Riebe, C. S., Kirchner, J. W., and Finkel, R. C., 2003.Long-term rates of chemical weathering and physical erosion from cosmogenic nuclides and geochemical mass balance.*Geochim.Cosmochim.Acta* **67**, 4411-4427.

Riebe, C.S., Kirchner, J.W., Finkel, R.C., 2004. Erosional and climatic effects on long-term chemical weathering rates in granitic landscapes spanning diverse climate regimes. *Earth Planet. Sci. Lett.* **224**, 547–562.

Roller, S., Wittmann, H., Kastowski, M., and Hinderer, M., 2012.Erosion of the Rwenzori Mountains, East African Rift, from in situ-produced cosmogenic Be-10.*J. Geophys. Res.-Earth Surf.* **117**, 20.

Royne, A., Jamtveit, B., Mathiesen, J., and Malthe-Sorenssen, A., 2008.Controls on rock weathering rates by reaction-induced hierarchical fracturing.*Earth Planet. Sci. Lett.* **275**, 364-369.

Sak, P.B., Navarre-Sitchler, A.K., Miller, C.E., Daniel, C.C., Gaillardet, J., Buss, H.L., Lebedeva, M.I., Brantley, S.L., 2010. Controls on rind thickness on basaltic andesite clasts weathering in Guadeloupe. *Chem. Geol.* **276**, 129–143.

Sak, P.B., Fisher, D.M., Gardner, T.W., Murphy, K., Brantley, S.L., 2004. Rates of weathering rind formation on Costa Rican basalt. Geochimica et Cosmochimica Acta68, 1453–1472.

Schulz, M.S., White, A.F., 1999. Chemical weatheringin a tropical watershed, Luquillo mountains, Puerto Rico III: Quartz dissolution rates. *Geochim. Cosmochim.Acta* **63**, 337-350.

Silva, E. I. L. and Manuweera, L., 2004.Surface and rainwater chemistry of Sri Lanka - a risk of acidification.*Asian J. of Water, Environment and Pollution* **1**, 79-86.

Turner, B.F., Stallard, R.F., and Brantley, S.L., 2003.Investigation of in situ weathering of quartz diorite bedrock in the Rio Icacos basin, Luquillo experimental forest, Puerto Rico.*Chem. Geol.* **202**, 313-341.

Vanacker, V., von Blanckenburg, F., Hewawasam, T., and Kubik, P. W., 2007a. Constraining landscape development of the Sri Lankan escarpment with cosmogenic nuclides in river sediment.*Earth Planet. Sci. Lett.* **253**, 402-414.

Vanacker, V., von Blanckenburg, F., Govers, G., Molina, A., Poesen, J., Deckers, J., and Kubik, P. W., 2007b. Restoring dense vegetation can slow mountain erosion to near natural benchmark levels. *Geology* **35**, 303-306.

von Blanckenburg, F., 2005. The control mechanisms of erosion and weathering at basin scale from cosmogenic nuclides in river sediment (Frontiers Article). *Earth Planet. Sci. Lett.* **237**, 462-479.

von Blanckenburg, F., Hewawasam, T., Kubik, W.P., 2004. Cosmogenic nuclide evidence for low weathering and denudation in the wet, tropical highlands of Sri Lanka. *J. Geophys. Res.* **109**, F03008.

Weerakkody, J., Parkinson, D., 2006a. Input, accumulation and turnover of organic matter, nitrogen and phosphorus in surface organic layers of an upper montane rainforest in Sri Lanka. *Pedobiologia* **50**, 377-383.

Weerakkody, J., Parkinson, D., 2006b. Leaf litter decomposition in an upper montane rainforest in Sri Lanka. *Pedobiologia* **50**, 387-395.

West, A.J., Galy, A., Bickle, M., 2005. Tectonic and climatic controls on silicate weathering. *Earth Planet. Sci. Lett.* **235**, 211–228.

White A. F. and Brantley S. L. (2003) The effect of time on the weathering of silicate minerals: why do weathering rates differ in the laboratory and field? Chem. Geol. 202, 479–506.

White, A. F., 2002. Determining mineral weathering rates based on solid and solute weathering gradients and velocities: application to biotite weathering in saprolites. *Chem. Geol.* **190**, 69-89.

Table 1 Mineral composition and modal mineralogy of charnockite bedrock at Hakgala

Mineral	**Mineral composition (EDX)**	**Charnockite bedrock at Hakgala**		**Charnockite at Kurunegala (Burton and O'Nions, 1990)**
		Modal mineralogy (vol%) (CIPW norm calculation)	Modal mineralogy (vol%) (500 point counts)	Modal mineralogy (vol%) (10,000 point counts)
Quartz	SiO_2	23	30	30.3
Plagioclase	$Si_{2.75}Al_{1.25}Na_{0.75}Ca_{0.25}O_8$	45	25	33.2
K feldspar	$Si_3Al_1K_{0.8}Na_{0.2}O_8$	25	32	27.8
Orthopyroxene	$Si_{1.8}Mg_{0.8}Fe_{1.0}O_6$	4	4	3.1
Biotite	$Si_{2.7}Al_{1.1}K_{0.7}Mg_{1.2}Fe_{1.0}Ti_{0.2}O_{10}(OH)_2$	n.d.*	7	1.5
Hornblende		n.d.*	accessory	0.6
Ilmenite, Magnetite		accessory	accessory	3.0
Apatite		accessory	accessory	0.36
Zircon		accessory	accessory	0.04
Allanite		accessory	accessory	<0.02

Data are from Hakgala (this study). Data from Burton and O'Nions (1990) at Kurunegala (northwestern Sri Lanka) are shown for comparison. The large difference between point-counting and CIPW norm calculation for Hakgala stems from the fact that some Na is hosted in K-feldspar, a feature not accounted for by CIPW norm calculation.* hydrous minerals are ignored in the CIPW norm calculation.

Table 2 Major minerals in surface soil, upper saprolite and lower saprolite of the weathering profile as identified by XRD analyses of bulk samples.

Type	Depth (cm)	Major minerals
Surface soil	0-30	quartz, goethite, kaolinite
	30-60	quartz, goethite, kaolinite
Upper saprolite	125-150	quartz, goethite, kaolinite
	220-250	quartz, goethite, kaolinite
	300-320	quartz, goethite, kaolinite
Lower saprolite	800-820	quartz, biotite, plagioclase, K-feldspar, goethite, kaolinite
	985-1020	quartz, biotite, plagioclase, K-feldspar, goethite, kaolinite

Table 3 Measured elemental concentrations of bedrock (charnockite) at Hakgala, and comparison with two other charnockite locations at Kurunegala and metasedimentary rocks in crystalline crust of Sri Lanka.

Sample name	SiO_2 (wt%)	TiO_2 (wt%)	Al_2O_3 (wt%)	Fe_2O_3 (wt%)	MnO (wt%)	MgO (wt%)	CaO (wt%)	Na_2O (wt%)	K_2O (wt%)	P_2O_5 (wt%)	LOI (wt%)	Sum (wt%)
Charnockite - Hakgala												
SL61 Hak2010 1090cm	66.8	0.519	15.7	3.55	0.043	1.18	2.75	3.91	3.87	0.181	1.11	99.63
SL63 Hak2010 P+18m	66.9	0.577	15.4	4.04	0.049	1.52	2.86	4.07	3.09	0.207	0.79	99.55
SL64 Hak2010 P-20m	66.4	0.453	16.4	2.78	0.030	1.01	2.15	3.77	5.48	0.144	0.91	99.56
SL65 Hak2010 P+1m	68.0	0.563	15.0	3.59	0.046	1.29	2.62	3.74	3.70	0.184	0.91	99.63
SL66 Hak2010 P+22m	66.9	0.564	15.2	3.76	0.044	1.41	2.78	3.84	4.08	0.188	0.81	99.58
SL68 Hak2010 P 1030cm	68.1	0.521	15.1	3.51	0.035	1.05	2.21	3.21	3.85	0.172	1.92	99.64
SL69 Hak2010 P-1125cm	67.7	0.547	15.2	3.57	0.041	1.35	2.67	3.7	3.76	0.180	0.83	99.59
SL70 Hak2010 P-3m	67.0	0.525	15.4	3.66	0.053	1.32	2.69	3.71	3.91	0.174	1.15	99.64
SL71 Hak2010 P-40m	68.1	0.506	14.9	3.18	0.043	0.95	2.31	3.63	4.21	0.172	1.59	99.64
Average	*67.4*	*0.531*	*15.4*	*3.52*	*0.043*	*1.23*	*2.56*	*3.73*	*3.99*	*0.178*	*1.11*	*99.61*
Standard Deviation	*0.7*	*0.04*	*0.5*	*0.36*	*0.01*	*0.20*	*0.27*	*0.24*	*0.64*	*0.017*	*0.40*	
Charnockite – Kurunegala (Hansen, 1987)												
Average (n=7)	*70.3*	*0.48*	*14.5*	*3.12*	*0.07*	*0.75*	*2.28*	*3.30*	*4.52*	*0.14*	*0.33*	*99.43*
Standard Deviation	*0.7*	*0.04*	*0.3*	*0.26*	*0.02*	*0.18*	*0.15*	*0.32*	*0.36*	*0.02*	*0.20*	
Charnockite – Kurunegala (Burton and O'Nions, 1990)	70.4	0.48	14.5	3.56	0.09	0.92	2.39	3.25	4.05	0.15	0.20	99.98
Metasedimentary Rocks (Prame, 1994)												
Average (n=23)	*65.2*	*0.82*	*16.6*	*7.25*	*0.19*	*2.1*	*1.84*	*2.52*	*3.29*	*0.08*	*-*	*99.91*
Standard Deviation	*5.2*	*0.38*	*1.6*	*3.12*	*0.19*	*1.01*	*0.64*	*0.77*	*0.82*	*0.05*	*-*	

Table 3-continued

Sample name	Ba (µg/g)	Cr (µg/g)	Ga (µg/g)	Nb (µg/g)	Ni (µg/g)	Rb (µg/g)	Sr (µg/g)	V (µg/g)	Y (µg/g)	Zn (µg/g)	Zr (µg/g)
Charnockite - Hakgala											
SL61 Hak2010 1090cm	1072	14	18	12	11	126	408	53	30	50	227
SL63 Hak2010 P+18m	867	19	20	11	18	114	385	61	26	57	229
SL64 Hak2010 P-20m	1539	18	20	11	16	172	440	36	32	47	192
SL65 Hak2010 P+1m	982	15	18	12	17	134	390	51	29	54	242
SL66 Hak2010 P+22m	1099	18	20	12	17	141	412	52	34	48	238
SL68 Hak2010 P 1030cm	1134	13	19	11	13	133	373	54	27	47	216
SL69 Hak2010 P-1125cm	1090	18	19	<10	18	129	403	54	29	45	222
SL70 Hak2010 P-3m	1048	17	18	12	17	127	405	56	29	50	214
SL71 Hak2010 P-40m	1020	17	19	14	11	126	361	40	38	51	232
Average	*1095*	*17*	*19*	*12*	*15*	*134*	*397*	*51*	*30*	*50*	*224*
Standard Deviation	*184*	*2.1*	*1*	*1*	*3*	*16*	*23*	*8*	*4*	*4*	*15*
Charnockite – Kurunegala (Hansen, 1987)											
Average (n=7)	*995*	*16*	-	*16*	*2*	*155*	*370*	*34*	*20*	*39*	*221*
Standard Deviation	*153*	*2*	-	*4*	*0*	*35*	*57*	*6*	*6*	*1*	*20*
Charnockite – Kurunegala (Burton and O'Nions, 1990)	833	18	-	17	<2	-	-	25	19	39	198
Metasedimentary Rocks (Prame, 1994)											
Average (n=23)	*779*	*90*	*22*	*11*	*43*	*81*	*209*	*99*	*36*	*106*	*214*
Standard Deviation	*344*	*47*	*4*	*4*	*31*	*61*	*93*	*59*	*14*	*52*	*70*

Analytical uncertainties for XRF data analyzed in this study are better than 0.5% (relative) for major elements and 10% for trace elements.
Detection limits for trace elements are at 10 µg/g for all elements, except Ba, where the detection limit is at 20 µg/g.

Table 4 Elemental concentrations in soil and saprolite samples and CDF from the regolith profile at Hakgala.

Sample name	Depth (cm)	SiO_2 (wt%)	TiO_2 (wt%)	Al_2O_3 (wt%)	Fe_2O_3 (wt%)	MnO (wt%)	MgO (wt%)	CaO (wt%)	Na_2O (wt%)	K_2O (wt%)	P_2O_5 (wt%)	LOI (wt%)	Sum (wt%)
Soil													
SL6 Hak 2010 soil	0-30	53.1	1.617	13.4	7.25	0.034	0.38	0.19	<0.01	0.46	0.117	23.19	99.69
SL7 Hak 2010 soil	30-60	61.0	1.666	15.5	8.90	0.050	0.41	0.14	0.06	0.48	0.099	11.39	99.70
SL30 Hak 2010 soil 1	0-20	50.9	1.261	14.7	9.26	0.038	0.40	0.29	<0.01	0.27	0.146	22.45	99.70
SL31 Hak 2010 soil 1	20-40	52.3	1.361	15.1	10.81	0.036	0.37	0.22	0.06	0.27	0.145	18.90	99.61
SL32 Hak 2010 soil 1	40-60	54.2	1.195	14.6	13.95	0.045	0.32	0.15	<0.01	0.22	0.142	15.00	99.78
SL33 Hak 2010 soil 2	0-20	49.1	1.264	14.7	8.71	0.037	0.45	0.39	<0.01	0.29	0.155	24.61	99.70
SL34 Hak 2010 soil 2	20-40	53.2	1.311	14.7	10.16	0.036	0.45	0.3	<0.01	0.27	0.136	19.24	99.71
SL35 Hak 2010 soil 2	40-60	49.7	1.193	13.2	10.70	0.043	0.51	0.37	0.02	0.27	0.123	23.64	99.71
SL36 Hak 2010 soil 3	0-20	52.7	1.239	13.7	8.31	0.035	0.43	0.4	0.04	0.30	0.143	22.41	99.67
SL37 Hak 2010 soil 3	20-40	54.2	1.313	15.1	10.48	0.038	0.45	0.29	0.12	0.30	0.133	17.27	99.73
SL38 Hak 2010 soil 3	40-60	54.8	1.344	14.6	11.67	0.041	0.4	0.27	<0.01	0.28	0.135	16.21	99.72
SL88 Hak 2010-combined soil 1+2+3	40-60	52.6	1.312	14.8	10.43	0.039	0.39	0.27	0.92	0.31	0.138	18.22	99.43
SL89 Hak 2010-combined soil 1+2+3	20-40	55.1	1.234	14.0	12.71	0.037	0.41	0.27	0.6	0.29	0.144	14.76	99.56
SL90 Hak 2010-combined soil 1+2+3	0-20	44.3	1.158	12.7	7.56	0.033	0.38	0.33	0.24	0.27	0.132	32.56	99.65
Average		*52.6*	*1.319*	*14.3*	*10.06*	*0.039*	*0.41*	*0.28*	*0.15*	*0.31*	*0.135*	*20.00*	*99.67*
Standard Deviation		*3.7*	*0.149*	*0.8*	*1.90*	*0.005*	*0.05*	*0.08*	*0.27*	*0.07*	*0.014*	*5.32*	
Saprolite													
SL8 Hak 2010	60-100	62.6	1.785	21.6	12.16	0.038	0.4	0.07	0.05	0.51	0.128	0.27	99.55
SL9Hak 2010	100-125	56.7	1.277	18.2	11.23	0.052	0.26	0.06	0.06	0.39	0.108	11.27	99.66
SL10 Hak 2010	125-150	35.7	1.084	18.8	11.02	0.058	0.17	0.01	<0.01	0.29	0.089	32.53	99.80
SL11 Hak 2010	150-220	49.0	0.977	25.1	11.04	0.070	0.31	0.01	0.24	0.38	0.083	12.37	99.61
SL12 Hak 2010	220-250	24.6	0.573	10.1	4.44	0.066	0.2	<0.01	0.07	0.35	0.034	59.39	99.83
SL13 Hak 2010	250-300	50.3	1.117	22.7	12.08	0.114	0.74	0.01	0.21	1.19	0.143	10.89	99.52
SL14 Hak 2010	300-320	68.6	0.183	13.8	9.18	0.142	0.12	0.02	<0.01	0.25	0.169	7.31	99.73
SL15 Hak 2010	320-360	60.0	0.925	20.1	7.81	0.100	0.47	0.01	<0.01	0.96	0.096	9.25	99.77
SL16 Hak 2010	360-410	63.4	0.685	20.0	5.24	0.050	0.86	0.02	<0.01	0.95	0.112	8.5	99.83
SL17 Hak 2010	410-460	62.5	0.725	20.3	5.11	0.036	0.54	0.01	0.21	0.85	0.079	9.23	99.62
SL18 Hak 2010	460-500	61.2	0.672	21.4	4.64	0.055	0.74	0.03	0.09	1.74	0.075	8.94	99.64
SL19 Hak 2010	500-550	60.3	0.706	20.7	4.48	0.026	0.76	0.03	0.40	3.28	0.125	8.68	99.53
SL20 Hak 2010	550-600	55.8	0.826	24.3	4.49	0.016	0.91	0.02	0.11	3.03	0.108	9.89	99.54
SL21 Hak 2010	600-650	61.7	0.740	20.5	4.61	0.024	0.75	0.02	0.37	2.90	0.142	7.8	99.50
SL22 Hak 2010	650-700	51.5	0.689	16.5	4.04	0.025	0.72	0.06	0.13	2.52	0.136	23.36	99.69
SL23 Hak 2010	700-750	58.5	0.811	20.5	5.12	0.026	0.85	0.16	0.55	4.19	0.222	8.64	99.50

SL24 Hak 2010	750-800	58.4	0.771	21.0	4.82	0.036	0.84	0.13	0.33	3.97	0.214	9.02	99.53
SL25 Hak 2010	800-820	63.0	0.638	18.9	3.92	0.019	0.79	0.58	1.10	4.86	0.164	5.63	99.54
SL26 Hak 2010	850-885	62.1	0.629	19.0	4.65	0.030	0.82	0.25	0.58	4.51	0.203	6.77	99.56
SL27 Hak 2010	955-970	60.4	0.649	20.2	5.06	0.132	0.94	0.64	1.04	3.50	0.201	6.91	99.59
SL28 Hak 2010	970-995	60.7	0.693	21.0	5.02	0.065	0.71	0.04	0.08	3.36	0.106	7.91	99.64
SL29 Hak 2010	985-1020	76.0	0.348	12.7	2.65	0.029	0.45	0.03	0.04	2.55	0.052	5.01	99.83
SL67 Hak 2010 P	1020	62.5	0.740	19.7	4.28	0.053	0.92	0.04	0.41	3.83	0.091	7.01	99.51
Average		*57.6*	*0.793*	*19.4*	*6.40*	*0.055*	*0.62*	*0.10*	*0.26*	*2.19*	*0.13*	*12.03*	*99.63*
Standard Deviation		*10.5*	*0.317*	*3.5*	*3.04*	*0.036*	*0.27*	*0.17*	*0.31*	*1.57*	*0.05*	*12.12*	
Corestone													
SL48 Hak 2010 Zone 2	830	68.5	0.510	15.0	3.35	0.037	1.24	2.48	3.77	3.65	0.170	0.83	99.57
SL51 Hak 2010 Zone 3	830	68.3	0.478	15.0	2.98	0.025	0.98	2.26	3.56	4.29	0.194	1.59	99.65
SL54 Hak 2010 Zone 4	830	66.5	0.629	16.3	3.80	0.013	0.88	1.4	2.36	4.63	0.265	2.93	99.65

Table 4- continued

Sample name	**Ba (µg/g)**	**Cr (µg/g)**	**Ga (µg/g)**	**Nb (µg/g)**	**Ni (µg/g)**	**Rb (µg/g)**	**Sr (µg/g)**	**V (µg/g)**	**Y (µg/g)**	**Zn (µg/g)**	**Zr (µg/g)**	**CDF (Zr)**
Soil												
SL6 Hak 2010 soil	140	102	19	28	36	34	45	141	14	76	448	0.61
SL7 Hak 2010 soil	159	116	21	36	41	35	45	166	15	80	477	0.58
SL30 Hak 2010 soil 1	121	105	19	24	63	39	34	158	<10	72	358	0.51
SL31 Hak 2010 soil 1	113	122	22	24	36	38	28	171	<10	75	350	0.48
SL32 Hak 2010 soil 1	120	173	20	21	33	35	22	190	<10	76	341	0.44
SL33 Hak 2010 soil 2	127	101	21	26	36	40	43	146	<10	70	371	0.54
SL34 Hak 2010 soil 2	131	139	22	22	34	34	33	163	<10	74	315	0.42
SL35 Hak 2010 soil 2	140	125	21	20	33	31	31	171	<10	72	441	0.61
SL36 Hak 2010 soil 3	144	99	20	23	37	38	41	141	<10	65	339	0.48
SL37 Hak 2010 soil 3	151	139	22	26	38	40	36	162	<10	70	350	0.47
SL38 Hak 2010 soil 3	145	132	21	29	37	36	30	178	<10	68	307	0.38
SL88 Hak 2010-combined soil 1+2+3	143	134	22	22	36	37	32	167	<10	76	361	0.49
SL89 Hak 2010-combined soil 1+2+3	126	134	22	21	33	31	30	188	<10	69	395	0.51
SL90 Hak 2010-combined soil 1+2+3	108	91	16	18	29	29	34	126	<10	61	311	0.51
Average	*133*	*122*	*21*	*24*	*37*	*36*	*35*	*162*	*15*	*72*	*369*	*0.50*
Standard Deviation	*15*	*22*	*2*	*5*	*8*	*4*	*7*	*18*	*1*	*5*	*53*	*0.07*
Saprolite												
SL8 Hak 2010	162	146	33	37	61	48	39	203	16	84	726	0.69
SL9Hak 2010	120	144	25	28	81	33	31	174	12	74	479	0.58
SL10 Hak 2010	84	183	27	22	44	32	14	158	12	74	284	0.46
SL11 Hak 2010	75	180	36	22	57	46	12	157	12	79	297	0.33

SL12 Hak 2010	64	88	13	16	20	33	<10	75	<10	32	186	0.51
SL13 Hak 2010	245	185	27	22	59	178	19	172	22	93	388	0.48
SL14 Hak 2010	122	164	16	5	42	23	14	105	26	66	1368	0.85
SL15 Hak 2010	431	132	26	21	73	210	33	112	18	92	289	0.29
SL16 Hak 2010	309	51	27	15	28	181	35	73	15	99	287	0.28
SL17 Hak 2010	291	22	28	20	30	133	33	62	15	79	301	0.32
SL18 Hak 2010	595	14	25	19	36	152	85	63	17	84	250	0.18
SL19 Hak 2010	965	16	24	18	32	192	164	57	19	82	297	0.30
SL20 Hak 2010	982	15	27	18	44	208	160	68	18	110	267	0.24
SL21 Hak 2010	988	17	23	18	30	150	178	59	19	88	344	0.39
SL22 Hak 2010	744	13	20	14	21	112	123	59	17	68	318	0.46
SL23 Hak 2010	1241	19	25	19	38	163	201	73	15	80	323	0.36
SL24 Hak 2010	1175	24	26	18	33	168	188	74	14	70	295	0.30
SL25 Hak 2010	1467	20	22	14	24	176	285	61	26	73	236	0.10
SL26 Hak 2010	1342	19	25	18	33	174	234	62	16	75	241	0.13
SL27 Hak 2010	1324	24	24	14	40	161	231	60	76	110	234	0.10
SL28 Hak 2010	1170	23	24	17	30	161	183	63	103	106	324	0.36
SL29 Hak 2010	733	13	14	<10	14	144	143	28	49	42	149	0.00
SL67 Hak 2010 P	1333	17	24	15	35	166	183	63	65	127	299	0.30
Average	*694*	*67*	*24*	*18*	*39*	*132*	*118*	*91*	*27*	*82*	*356*	*0.35*
Standard Deviation	*500*	*67*	*5*	*7*	*17*	*63*	*88*	*48*	*24*	*21*	*247*	*0.20*
Corestone												
SL48 Hak 2010 Zone 2	967	18	19	10	29	135	379	55	29	85	223	0.00
SL51 Hak 2010 Zone 3	1180	13	19	<10	15	149	388	47	43	56	184	0.00
SL54 Hak 2010 Zone 4	1371	14	20	13	18	157	333	56	20	51	224	0.02

Relative analytical uncertainties in concentrations measured by XRF are about 0.5% for major elements and about 10% for trace elements. Error propagation then leads to a relative uncertainty estimate of about 14% for CDF values.

Table 5 Sr isotope ratios in bedrock, saprolite and soil samples from the regolith profile at Hakgala.

Sample	Depth (cm) of soil/saprolite or type of sample	$^{87}Sr/^{86}Sr$	2 S.D.	n
SL88 Hak 2010	40-60	0.71813	0.00004	3
SL89 Hak 2010	20-40	0.71850	0.00002	3
SL90 Hak 2010	0-20	0.71885	0.00002	3
SL8 Hak 2010	60-100	0.72890	0.00003	3
SL16 Hak 2010	360-410	0.76449	0.00004	3
SL19 Hak 2010	500-550	0.75453	0.00005	6
SL21 Hak 2010	600-650	0.75327	0.00003	6
SL23 Hak 2010	700-750	0.75692	0.00002	6
SL26 Hak 2010	850-885	0.74894	0.00002	6
SL29 Hak 2010	985-1020	0.74530	0.00001	3
SL48 Hak 2010 Zone 2	Corestone Zone 2	0.74017	0.00004	6
SL51 Hak 2010 Zone 3	Corestone Zone 3	0.74279	0.00002	6
SL54 Hak 2010 Zone 4	Corestone Zone 4	0.74653	0.00003	6
SL63 Hak 2010 P+18m	Bedrock	0.73881	0.00002	6
SL69 Hak 2010 P-1125cm	Bedrock	0.73737	0.00004	6

Table 6 Saprolite and soil density measured from horizontal cores, and associated strain calculated from Zr and Ti concentrations (ε_{Zr} and ε_{Ti}) in the neighbouring saprolite samples (Table 4) following the approach of Brimhall and Dietrich (1987) (equation 1). The deepest saprolite sample displays large values of strain despite our direct observations that weathering is almost isovolumetric at this depth. This result is hence considered to be an outlier. For these calculations, bedrock density was assumed to be 2700 kg m^{-3}.

Core	Depth (cm) of soil/saprolite	Density (kg m^{-3})	ε_{Zr}	ε_{Ti}
HA2010 Soil 0-15 cm	0-15	1096	0.78	0.13
HAK2010210cm	210	1362	0.50	0.08
HAK2010340cm	340	1509	0.39	0.03
HAK2010380cm	380	1536	0.37	0.36
HAK2010976cm	976	1852	0.01	0.12
HAK2010986cm	986	1775	1.29	1.32

Table 7 Denudation and weathering rates for the regolith profile at Hakgala and for the large river catchments in the Central Highlands of Sri Lanka

Estimates at 10^4 yearstime scale			**Estimates at 10^1 yearstime scale**				
Sample name	Cosmogenic nuclide derived denudation rate		Catchment	Cationic yield ($t\ km^{-2}y^{-1}$)	Silicate-derived cationic yield ($t\ km^{-2}y^{-1}$)	Silicate-derived oxide yield ($t\ km^{-2}\ y^{-1}$)	Weathering rate ($mm\ y^{-1}$)
HG(F)-3 (sed)	10.8 ± 0.7 mm ky^{-1}		Atabage Oya (AO)	50	27	28	9.9-10.6
HG(F)-3e (soil)	11.4 ± 0.8 mm ky^{-1}		Belihul Oya (BO)	56	30	31	11.0-11.7
HG(F)-4e (sed)	10.9 ± 0.7 mm ky^{-1}		Huluganga (HUG)	27			
HG(F)-4e (soil)	7.9 ± 0.6 mm ky^{-1}		Maha Oya (MO)	67	34	36	12.6-13.5
			Nilambe Oya (NO)	35	22	23	8.0-8.5
Mean rate ± SD	10.3 ± 1.4 mm ky^{-1}		Uma Oya (UO)	38	16	18	6.1-6.7
	27.8 ± 3.8 t $km^{-2}\ y^{-1}$		Peradeniya (M-PER)	39			
$[Zr]_{saprolite}/[Zr]_{bedrock}$ 1.5							
Total corr denudation rate	15.5 $mmky^{-1}$						
	41.9 t $km^{-2}\ y^{-1}$						
Mean CDF	0.5						
Mean corrr weathering rate	8 $mmky^{-1}$						
	21.6 t $km^{-2}\ y^{-1}$						

10^4y time scale estimates are from *in situ* cosmogenic nuclide-derived denudation rate and CDF. 10^1y time scale estimates are from river loads measured in streams of the Sri Lankan Highlands (Hewawasam et al., 2003; von Blanckenburg et al., 2004). Denudation rates of two top soil and two creek sediment in the close vicinity (within 200 m radius) of the regolith from Hewawasam et al. (2003) and von Blanckenburg et al. (2004) are considered in this study as representative. The abbreviations for catchments are shown in the location map of Figure 1A. Note that denudation rates from cosmogenic nuclides from Hewawasam et al. (2003) and von Blanckenburg et al.(2004) have been corrected for mass loss beneath the attenuation path length according to equation (3). Cationic yield here includes SiO_2. Sri Lankan carbonate contribution to dissolved Mg and Ca at the scale of these large rivers, most likely deriving from dolomitic marble fertilizers, was corrected for using a binary mixture model (section 4.4.2, Figure 8). For large rivers HUG and M-PER, for which dissolved chemical load reflects a three end member mixture (silicate weathering, carbonate and rock phosphate), silicate-derived cationic load and weathering rates were not calculated. Then, the contribution of rain and carbonate dust (as observed in topsoil) to the "pristine" component of the large river dissolved load was corrected for using the proportions determined by the full inversion of small, pristine creeks dissolved load data (section 4.4.1, Table 9). This correction affects Ca, Mg, Na, K but not SiO_2. The sum of all silicate-derived dissolved species is the silicate-derived cationic yield (which includes SiO_2 here), which was also converted to oxides ($CaO+MgO+Na_2O+K_2O+SiO_2$) to yield the silicate-derived oxide yield. Weathering rates, in $mm\ y^{-1}$, were calculated assuming a rock density of $2700kg\ m^{-3}$, and in two ways: using the river cationic yield and the oxide yield.

Table 8 Calculation of rates of advance of the weathering front at the spatial scales of the corestone and regolith profile, respectively, based on mineral weathering gradient (White, 2002). *Pl*, *Bt* and *Kfs* refer to plagioclase, biotite, and K-feldspar, respectively.

Parameter	**Weathering gradient[a,c]**	**Mass proportion of mineral in the source rock[b,c]**	**Mineral specific surface area[d]**	**Mineral weathering rate[e]**	**Rate of advance of the weathering front[f]**
Symbol (eq. 8-9)	$\Delta C_{min}/\Delta z$	$x_{min,r}$	S_{min}	R_{min}	w
Unit	$mol_{min}\ kg^{-1}_{bulk} m^{-1}$	$g_{min}\ g^{-1}_{bulk}$	$m^2_{min}\ g^{-1}_{min}$	$mol_{min}\ m^{-2}_{min}\ s^{-1}$	mm ky^{-1}
			Corestone		
min = Pl	5.44±0.98	0.34±0.13	1±0.3	$10^{-15}(10^{-16}$-$10^{-14})$	2 (0.14 -19)
				$10^{-14.6}$-$10^{-14.3}$	5-10
				10^{-13}	217
min = Bt	0.05-0.25	0.015-0.07	5±1.5	10^{-16} (10^{-17}-10^{-15})	0.06 (0.00 - 0.6)
				$10^{-13.1}$	48
			Regolith profile		
min = Kfs	0.002	0.30±0.03	1±0.3	10^{-18} (10^{-19}-10^{-17})	5 (0.4 - 43)

[a] $\Delta C_{Pl}/\Delta z$ was estimated using the average and standard deviation of the values obtained through $\Delta[Ca]/\Delta z$ and $\Delta[Na]/\Delta z$ across the corestone (Table 4), with zones 3 and 4 located at 10 cm and 15 cm from zone 2, respectively. The chemical composition of plagioclase (β in eq. 9) was taken from the EDX results (Table 2). The corresponding relative plagioclase loss from corestone zone 3 relative to zone 2 is around 20%, and 40% for zone 4 relative to zone 2. $\Delta C_{Kfs}/\Delta z$ was estimated using Sr concentration and isotope composition in the saprolite(between 10 m- and 3 m-depth) in eq. (11) and (12), which were solved for two unknowns: the mass fraction of biotite and K-feldspar ($x_{Bt,w}$ and $x_{Kfs,w}$), respectively. This calculation yields that throughout the saprolite, $x_{Bt,w}$ is between 1.9 and 0.4%, the latter value being reached at the top of the saprolite. $x_{Kfs,w}$ varies between 21% at the bottom of the saprolite, to 18% at 5 m-depth and 2% at the top of the saprolite. No uncertainty could be estimated for $\Delta C_{Kfs}/\Delta z$.

[b] We use a $x_{Pl,r}$ between 25% (volume-%from point-counting, Table 2) and 43% (weight-% from CIPW calculation, Table 2) to calculate an average and standard deviation. For $x_{Kfs,r}$ the estimates stem from our point-counting (32 vol%, Table 2) and Burton and O'Nions (1990)'s point counting (48% vol%).

[c] $\Delta C_{Bt}/\Delta z$ was estimated between zone 2 and zone 4 using Sr isotopes (eq. 12), assuming that ^{87}Sr is not released preferentially during Sr solubilisation. As K-feldspar does not weather in the corestone, its contribution to the Sr isotope signature is invariant, and the difference in $^{87}Sr/^{86}Sr$ between different zones is due to plagioclase and biotite weathering (pyroxene does not contribute significantly to the Sr budget in Sri Lankan charnockite, see section 4.1). Knowing the relative mass loss of plagioclase (see comment [a] of this table), the relative mass loss of biotite can be computed from eq. (12). This relative mass loss is translated into

biotite mass fraction, $x_{Bt,w}$ using two possible values for initial biotite mass fraction $x_{Bt,r}$: 1.5 vol% from Burton and O'Nions, 1990; and 7 vol% from our point-counting, Table 2. The resulting mass fraction was then converted into two values of $\Delta C_{Bt}/\Delta z$. However, as the value chosen for $x_{Bt,r}$ cancels out in the calculation of w (eq. 8), the choice of $x_{Bt,r}$ does not propagate any uncertainty.

[d] S_{min} estimates are from the typical values reported by White and Brantley (2003) with assumed relative uncertainties (63% confidence intervals) of 30%.

[e] R_{min} (dissolution rates) estimates were taken from different sources. First, for each mineral, the typical values reported by White and Brantley (2003) were used, with relative uncertainties (63% confidence intervals) assumed to be of one order of magnitude. For plagioclase, additional estimates by Turner et al. (2003) and Buss et al. (2008) from Puerto Rico are used. For biotite, we also apply the much faster biotite oxidation rate reported by Buss et al. (2008) from Puerto Rico, as Sr isotopes trace biotite oxidation rather than dissolution (see note [c] of this table and Blum and Erel, 1997).

[f] Uncertainties were calculated using a Monte-Carlo method for the estimates based on White and Brantley (2003)'s R_{min} estimates. As the uncertainties on $\Delta C_{min}/\Delta z$, $x_{min,r}$, and S_{min} are assumed to be normally distributed and R_{min} uncertainties are assumed to be log-normally distributed, the uncertainty on w does not follow a normal distribution. Therefore, we report the 63% confidence interval for w(in parenthesis), along with the most likely value, rather than a standard deviation. The very high value of corestone w inferred from Buss et al. (2008)'s plagioclase dissolution rate was not further considered.

Table 9 Parameters used for the determination of end member contribution to the dissolved load of the three small creeks sampled near the regolith profile at Hakgala in 2010-2011.

	A priori *values*				**A posteriori *values***			
Mass ratios	**Silicate weathering**	**Carbonate weathering**	**Rain water**	**Small creeks**	**Silicate weathering**	**Carbonate weathering**	**Rain water**	**Small creeks**
Si/Mg	28.3±3.0	0.001±0.001	0.001±0.001	4.40±1.60	28.1±3.0	0.001±0.001	0.001±0.001	4.81±1.41
Na/Mg	4.10±0.40	0.001±0.001	1.70±1.70	1.97±0.79	4.13±0.40	0.001±0.001	2.44±1.56	1.27±0.46
Ca/Mg	2.70±0.30	2.0±1.0	2.30±1.30	1.83±0.21	2.69±0.30	1.56±0.53	2.02±1.18	1.86±0.20
K/Mg	4.70±0.50	0.001±0.001	1.20±1.20	0.86±0.42	4.66±0.49	0.001±0.001	0.91±1.05	1.01±0.29
X_{Mg} (%)	**45±30**	**45±30**	**10±20**		**17±5**	**60±15**	**23±15**	
Si/Ca	10.3±1.0	0.001±0.001	0.001±0.001	2.43±0.92	10.15±0.98	0.001±0.001	0.001±0.001	2.89±0.76
Na/Ca	1.50±0.20	0.001±0.001	0.65±0.37	1.10±0.51	1.52±0.20	0.001±0.001	0.71±0.36	0.60±0.16
Mg/Ca	0.36±0.05	1.00±0.20	0.60±0.40	0.55±0.08	0.36±0.05	0.57±0.18	0.68±0.34	0.54±0.07
K/Ca	1.66±0.20	0.001±0.001	0.54±0.40	0.47±0.21	1.63±0.20	0.001±0.001	0.46±0.38	0.57±0.14
X_{Ca} (%)	**65±30**	**25±30**	**10±20**		**28±8**	**49±16**	**23±16**	

A full inversion method was used to solve mixing equations (eq. 13) in order to estimate the contribution of (1) silicate weathering, (2) dissolution of a Ca- and Mg-rich material (called "topsoil carbonate"), and (3) rain water to Ca and Mg, following Négrel et al. (1993) and Gaillardet et al. (1999), on the small creeks dissolved loads. The *a priori* values for the "silicate weathering" end member are based on eq. 8, in which the chemical composition of water resulting from silicate weathering throughout the Hakgala profile, was calculated by comparing bedrock and upper saprolite chemical composition. *A priori* relative uncertainties were taken to be 10 to 15%. Congruent dissolution was assumed for the weathering of the "topsoil carbonate" end member, and the Ca/Mg ratio was assumed to be 2.0 (±1.0), as observed in the Hakgala profile topsoil. This end member does not contain any K, Na, nor Si. The "rain water" end member was estimated from data reported on rain water chemical composition in the Sri Lankan Highlands by Silva and Manuweera (2004), using only the dataset from the 1900-3200 m-altitude domain. As these authors only report maximum and minimum concentrations for the two altitude domains, only four concentration data for each element are available, over which the average and standard deviation were calculated to estimate *a priori* values and associated uncertainties. For the "small creeks" mixture, averages and standard deviations of the concentration data measured during three sampling campaigns in 2010-2011 (Table S2, n=8 for each element, since sample HAK2010-S3-3 was excluded) were used. The results of the inversion ("*a posteriori* values") yield the contribution of Ca and Mg of each of these end members, with lower *a posteriori* than *a priori* uncertainties. Similarly, the *a posteriori* uncertainties are lower for the end members. This comparison indicates that information was actually gained during the inversion. The only end member of which the chemical composition has to be modified significantly in order to solve the system is the "rain water" end member.

Supplementary Data

Table S1 Solute loads monitored in six tributaries and one main trunk of Mahaweli River within the Upper Mahaweli Catchment. Monthly discharge data are from the Mahaweli Authority of Sri Lanka.

Sample name	Sampling Date	Mean Monthly Discharge (10^6*m^3)	Measured Concentration of Solute Load (mg L^{-1})				
			Mg	Ca	K	Na	SiO_2
Atabageoya (basin area 43.5 km^2)							
AO-W-1	20-Mar-00	2.54	2.8	5.6	1.18	3.5	9.8
AO-W-2	2-Sep-00	7.76	2.3	9.1	1.16	2.3	11
AO-W-3	2-Oct-00	11.37	2.5	26	2.52	3.1	9.8
AO-W-4	7-Nov-00	11.39	3.0	7.0	1.15	2.5	12
AO-W-5	3-Dec-00	6.68	3.3	17	1.38	2.6	13
AO-W-6	7-Jan-01	5.55	3.1	5.0	1.03	2.4	12
AO-W-7	7-Feb-01	3.82	2.8	5.0	1.15	2.3	11
AO-W-8	4-Mar-01	2.54	3.9	8.6	1.06	2.8	14
AO-W-9	8-Apr-01	4.26	3.6	7.0	1.25	2.8	13
AO-W-10	20-May-01	7.19	4.0	9.8	1.16	2.8	14
AO-W-11	5-Jun-01	4.77	3.5	6.9	1.17	2.7	13
AO-W-12	1-Jul-01	5.21	3.2	6.1	0.97	2.4	12
Belihuloya (146 km^2)							
BO-W-1	20-Mar-00	6.32	6.4	16	1.22	5.0	17
BO-W-2	2-Sep-00	7.47	5.9	23	1.04	4.0	22
BO-W-3	2-Oct-00	13.96	6.6	17	1.06	4.2	23
BO-W-4	7-Nov-00	16.41	6.7	21	1.46	3.7	24
BO-W-5	3-Dec-00	18.82	6.4	15	1.09	3.5	25
BO-W-6	7-Jan-01	26.68	5.2	19	1.54	3.4	22
BO-W-7	7-Feb-01	16.11	4.7	10	1.11	3.1	21
BO-W-8	4-Mar-01	6.32	8.3	19	1.14	4.5	28
BO-W-9	8-Apr-01	8.29	7.8	19	2.10	4.2	27
BO-W-10	20-May-01	7.34	9.7	27	1.71	5.1	34
BO-W-11	5-Jun-01	7.90	7.7	19	1.40	4.2	29

BO-W-12	1-Jul-01	6.80	9.2	21	1.13	4.7	33
Huluganga (123 km^2)							
HUG-W-1	15-Mar-00	3.41	1.7	3.6	0.92	3.7	10
HUG-W-2	2-Sep-00	12.37	1.4	7.2	1.05	3.0	9.6
HUG-W-3	2-Oct-00	24.35	1.8	18	1.66	3.3	11
HUG-W-4	7-Nov-00	18.86	1.7	4.0	0.92	2.5	11
HUG-W-5	3-Dec-00	20.12	1.6	14	1.44	2.5	11
HUG-W-6	7-Jan-01	24.91	1.3	3.5	0.83	2.3	10
HUG-W-7	7-Feb-01	9.68	1.2	3.5	0.86	2.2	11
HUG-W-8	4-Mar-01	3.41	2.3	5.6	1.07	2.9	13
HUG-W-9	8-Apr-01	5.52	1.9	3.8	1.24	2.6	11
HUG-W-10	20-May-01	5.52	2.1	4.5	0.96	2.7	12
HUG-W-11	5-Jun-01	6.49	1.5	3.3	1.07	2.4	10
HUG-W-12	1-Jul-01	7.09	2.0	5.0	0.96	2.7	13
Mahaoya (107 km^2)							
MO-W-1	15-Mar-00	0.12	4.5	11	2.1	4.7	15
MO-W-2	2-Sep-00	6.79	3.6	9.8	1.15	4.5	20
MO-W-3	2-Oct-00	15.51	3.8	15	1.04	4.7	20
MO-W-4	7-Nov-00	24.75	5.3	18	1.80	4.2	22
MO-W-5	3-Dec-00	34.15	5.8	26	1.83	4.4	24
MO-W-6	7-Jan-01	10.06	5.0	12	1.17	3.8	21
MO-W-7	7-Feb-01	3.50	4.3	12	1.26	3.3	18
MO-W-8	4-Mar-01	0.12	8.9	31	1.84	5.3	27
MO-W-9	8-Apr-01	18.48	7.1	33	2.5	4.4	22
MO-W-10	20-May-01	8.36	10	28	2.4	5.3	30
MO-W-11	5-Jun-01	1.81	8.3	22	1.69	5.3	27
MO-W-12	1-Jul-01	2.56	8.6	26	1.61	5.4	28
Nilambeoya (62 km^2)							
NO-W-1	20-Mar-00	2.49	1.5	1.8	0.84	3.4	7.9
NO-W-2	2-Sep-00	5.51	2.4	4.0	1.12	3.6	12
NO-W-3	2-Oct-00	13.31	1.8	2.4	1.30	3.0	10
NO-W-4	7-Nov-00	13.23	2.4	6.8	1.17	2.8	13
NO-W-5	3-Dec-00	10.17	3.0	5.9	1.13	2.9	14
NO-W-6	7-Jan-01	5.66	3.3	6.9	2.1	3.1	13
NO-W-7	7-Feb-01	3.76	2.3	5.0	1.33	2.6	12
NO-W-8	4-Mar-01	2.49	3.5	13	1.96	3.5	15
NO-W-9	8-Apr-01	4.79	3.3	6.3	1.17	3.3	15
NO-W-10	20-May-01	5.36	3.1	7.0	1.10	3.2	15
NO-W-11	5-Jun-01	6.62	2.6	5.9	1.22	3.1	13

NO-W-12	1-Jul-01	5.76	3.2	7.2	1.15	3.3	15
Umaoya (98 km^2)							
UO-W-1	21-Mar-00	2.62	7.5	23	2.7	6.0	14
UO-W-2	2-Sep-00	3.18	7.0	45	5.2	5.4	18
UO-W-3	2-Oct-00	6.90	5.6	19	3.7	4.6	14
UO-W-4	7-Nov-00	9.32	7.0	37	4.3	4.6	18
UO-W-5	3-Dec-00	9.64	6.8	22	4.0	4.1	16
UO-W-6	7-Jan-01	7.21	8.4	26	3.8	4.8	20
UO-W-7	7-Feb-01	5.08	6.3	21	4.1	3.7	15
UO-W-8	4-Mar-01	2.62	8.0	34	4.2	5.3	30
UO-W-9	8-Apr-01	3.13	9.4	29	2.7	5.4	23
UO-W-10	20-May-01	4.17	8.7	29	2.7	5.4	23
UO-W-11	5-Jun-01	2.87	9.1	29	3.2	5.0	23
UO-W-12	1-Jul-01	2.29	7.7	26	4.4	5.5	19
Perdeniya (1167 km^2)							
M-PER-W-1	20-Mar-00	32.59	2.2	17	2.0	3.6	7.7
M-PER-W-2	2-Sep-00	208.59	1.7	6.9	1.15	2.9	10
M-PER-W-3	2-Oct-00	257.70	1.6	13	1.95	2.9	9.0
M-PER-W-4	7-Nov-00	336.65	2.1	6.2	1.30	2.3	10
M-PER-W-5	3-Dec-00	167.86	2.3	6.4	1.49	2.4	9.2
M-PER-W-6	7-Jan-01	71.46	2.2	6.3	1.66	2.5	9.4
M-PER-W-7	7-Feb-01	34.93	2.3	5.3	1.43	2.7	10
M-PER-W-8	4-Mar-01	32.59	2.2	5.2	1.48	2.5	9.0
M-PER-W-9	8-Apr-01	61.11	2.4	6.4	1.86	2.8	9.4
M-PER-W-10	20-May-01	137.99	2.1	5.7	2.0	2.6	9.0
M-PER-W-11	5-Jun-01	185.28	2.2	7.5	1.95	2.9	9.4
M-PER-W-12	1-Jul-01	241.41	1.70	4.0	1.26	2.2	8.6

Table S2 Surface water chemistry of creeks mostly ecologically pristine small catchments at Hakgala and shallow soil pore water chemistry in the regolith profile at Hakgala. Sample HAK-2010-S3-3 is thought to be influenced by domestic waste or fertilizer inputs and therefore was not considered for interpretation.

Sample name	Sampling Date	Depth (cm)	pH	Alkalinity (mg/L $CaCO_3$)	Mg (µg g^{-1})	Ca (µg g^{-1})	K (µg g^{-1})	Na (µg g^{-1})	SiO_2 (µg g^{-1})
Stream Water									
Agricultural Catchments:									
Perawella (basin areas <1km^2)	21-Mar-00	-	-	-	7.61	36.70	1.79	8.90	14.30
Pristine Catchments:									
Hakgala (basin area <1km^2)									
HAK-2000-S1-0	21-Mar-00	-	-	-	0.91	1.02	0.31	3.00	10.7
HAK-2000-S2-0	21-Mar-00	-	-	-	0.52	0.85	0.58	2.50	7.91
HAK-2010-S1-1	4-Oct-10	-	5.94	< 5	0.32	0.57	0.35	0.87	3.61
HAK-2010-S2-1	4-Oct-10	-	6.39	33	0.42	0.86	0.65	1.07	4.79
HAK-2010-S3-1	4-Oct-10	-	6.69	29	0.61	1.20	0.44	1.37	7.85
HAK-2011-S1-2	15-Feb-11	-	-	-	0.59	0.99	0.65	0.85	3.83
HAK-2011-S2-2	15-Feb-11	-	-	-	0.56	1.15	0.69	1.11	5.43
HAK-2011-S3-2	15-Feb-11	-	-	-	0.69	1.32	0.38	1.11	6.27
HAK-2011-S1-3	17-May-11	-	-	-	0.33	0.45	0.22	0.88	3.46
HAK-2011-S2-3	17-May-11	-	-	-	0.39	0.70	0.27	0.90	4.47
HAK-2011-S3-3	17-May-11	-	-	-	7.51	13.88	1.17	1.72	13.2
Shallow Soil Pore Water									
HAK2010-L1	5-Oct-10	107	-	21	0.45	0.76	0.29	0.94	7.38
HAK2010-L2	5-Oct-10	36	-	< 5	2.33	3.53	3.31	1.74	6.80
HAK2010-L3	5-Oct-10	70	-	37	0.41	0.57	1.44	1.06	7.06
HAK2010-L4	5-Oct-10	22	-	-	2.71	3.68	7.59	2.38	2.52
HAK2010-L5	5-Oct-10	36	-	-	0.71	1.01	0.87	1.42	9.26

Note: Threepristine creeks (denoted by -S1, -S2, and -S3) adjacent to the regolith profile at Hakgala were sampled at four different occasions (-0, -1, -2, -3). Sampling locations are shownin Figure 1c.